

A benchmark of first-principles methods for accurate prediction of semiconductor band gaps

Saeid Abedi,* Mehdi Tarighi Ahmadpour, Samira Baninajarian, Hamideh Kahnouji, and S. Javad Hashemifar†
Department of Physics, Isfahan University of Technology, Isfahan, 84156-83111, Iran

Zhong-Kang Han and Sergey V. Levchenko‡
Skolkovo Institute of Science and Technology, Bolshoy Boulevard 30/1, 121205 Moscow, Russia
(Dated: November 29, 2022)

The band gap is an important parameter of semiconductor materials that influences several functional properties, in particular optical properties. However, a fast and reliable first-principles prediction of band gaps remains a challenging problem. Standard DFT approximations tend to strongly underestimate band gaps, while the more accurate GW and hybrid functionals are much more computationally demanding and unsuitable for high-throughput screening. In this work, we have performed an extensive benchmark of several approximations with different computational complexity (G_0W_0 @PBEsol, HSE06, PBEsol, mBJ, PBEsol-1/2, and ACBN0) to evaluate and compare their performance in predicting the band gap of semiconductors. The benchmark is based on 114 binary semiconductors of different compositions and crystal structures, where about half of them have experimental band gaps. We find that, as expected, G_0W_0 @PBEsol performs well relative to the experiment, with a noticeable underestimation of the band gaps by about 14% on average. Surprisingly, G_0W_0 @PBEsol is followed closely by the much computationally cheaper pseudo-hybrid ACBN0 functional, showing an excellent performance with respect to experimental data. The meta-GGA mBJ functional also performs well relative to the experiment, even slightly better than G_0W_0 @PBEsol in terms of mean absolute (percentage) error. The HSE06 and PBEsol-1/2 schemes perform overall worse than ACBN0 and mBJ schemes but much better than PBEsol. Comparing the calculated band gaps on the whole data set (including the samples with no experimental band gap), we find that HSE06 and mBJ have excellent agreement with respect to the reference G_0W_0 @PBEsol band gaps. Thus, we propose the mBJ band gaps as economic descriptors when developing artificial intelligence models for high-throughput screening of semiconductor band gaps.

INTRODUCTION

A reliable prediction of the fundamental band gap of semiconductors and insulators, in contrast to their ground-state properties, is a challenging task for the Kohn-Sham density-functional theory (DFT) [1, 2]. It has been demonstrated recently that, although exact Kohn-Sham DFT does not reproduce fundamental gap, approximate DFT can in fact do it [3]. However, the accuracy of calculated band gaps is sensitive to the choice of exchange-correlation (xc) functional approximation. Conventional approximations, including the local density (LDA) [4] and generalized-gradient approximations (GGA) of Perdew, Burke, and Ernzerhof (PBE) [5], are not able to provide accurate band gaps because of the self-interaction error [4] and the absence of the derivative discontinuity [6–8]. The hybrid Heyd-Scuseria-Ernzerhof (HSE) functional [9, 10], meta-generalized gradient approximations (meta-GGAs) [11–13], DFT+ U [14, 15], DFT-1/2 [16–19], dynamical mean-field theory [20–22] and the many-body Green’s function based GW methods [23–25] are developed to address this problem.

A benchmark study on a group of elemental and binary semiconductors indicated a maximum error of about 0.7 eV in the band gaps obtained with the hybrid HSE03 functional, which is significantly better than the maximum error of more than 2 eV (approximately 50% for the relative error) for the

conventional PBE functional [4]. However, the non-local exact exchange term in the hybrid DFT schemes significantly increases the computational cost. Furthermore, the contribution of the exact exchange is controlled by an empirical hyperparameter in this approach. Our results give a mean absolute error of about 0.8 eV within HSE06. A more sophisticated scheme is the GW method, which is believed to be the most accurate approach for calculating the quasiparticle band gap of semiconductors and insulators [23]. However, this method is computationally very demanding [27] and thus is not suitable for high-throughput studies. In the current work, a mean absolute error of about 0.6 eV is predicted for this sophisticated scheme.

On the other hand, the DFT+ U approach provides a faster alternative for reliable prediction of the semiconductor band gaps. In this method, proper Hubbard U parameters provide the opportunity to correct the calculated band gaps relative to the experiment or more expensive methods, with a low computational cost comparable to the conventional DFT calculations. Nevertheless, the determination of the proper Hubbard parameters requires a nontrivial effort in this approach, involving additional DFT calculations in the framework of random-phase approximation (RPA) [28] and linear response approaches [29]. Recently, an alternative method was proposed for on-the-fly self-consistent computation of the Hubbard parameters – the ACBN0 pseudohybrid density functional. In ACBN0, a renormalization of the density matrix is employed to express the Hubbard parameters in terms of electron density to be determined during the self-consistent DFT calculations. We found no benchmark study of the band gaps within the DFT+ U scheme in the literature, which is likely because of the elaborating task of U determination.

* saeid.abedi@ph.iut.ac.ir

† hashemifar@iut.ac.ir

‡ s.levchenko@skoltech.ru

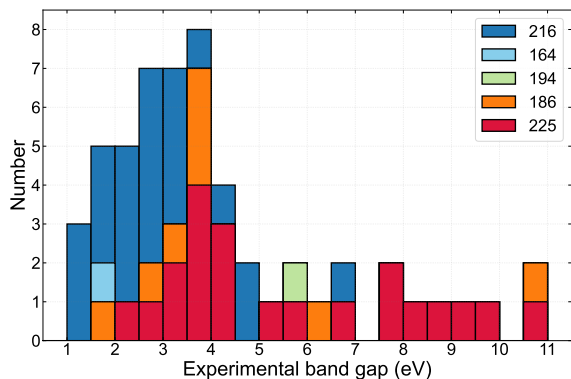


FIG. 1. Experimental band-gap distribution histogram of investigated binary compounds. Different colors represent different crystal structures. The space group numbers 216, 164, 194, 186, and 225 indicate $F\bar{4}3m$ (Zincblende), $P\bar{3}m1$ (Trigonal), $P6_3/mmc$ (Hexagonal), $P6_3mc$ (Wurtzite), $Fm\bar{3}m$ (Rocksalt) structures.

The modified Becke-Johnson potential (mBJ)[30] is another fast method for calculating the band gap of bulk solids. This method has been shown to have mean absolute errors between 0.47-0.5 eV (15-30% for the absolute relative error) when compared with experimental measurements [31, 32]. Our data indicate a high consistency between the mBJ and G_0W_0 methods with slightly better performance of mBJ in reproducing the experimental data.

Another computationally cheap approach for reliable band gap prediction is DFT-1/2 [16], which is a generalization of Slater’s half-occupation (transition state) technique [33, 34] for periodic solids by means of adding a local potential to the Kohn-Sham (KS) potential. This method provides approximate quasiparticle corrections to the band structure and consequently improves the band gap for a wide range of semiconductors and insulators at a low computational cost comparable to the standard DFT calculations [16]. The method has been applied to a number of test sets [17, 35, 36] and has been shown to have a mean absolute error (MAE) of 0.44 eV for LDA-1/2 and 0.67 eV for PBE-1/2 [19]. It also has been shown as a good starting point for G_0W_0 calculations [37].

In this paper, we report a benchmark study of band gaps of non-metallic compounds (with different structures) to compare the performance of a set of xc functionals, including ACBN0, HSE06, $G_0W_0@PBEsol$, mBJ, and $PBEsol-1/2$ methods. In order to construct our first-principles benchmark data set, we randomly selected a group of binary semiconductors from the Materials Project database [38]. The final data set has a size of 114 samples, where 56 compounds have experimental band gaps. The distribution of experimental band gaps is depicted in Fig. 1. It can be seen that the majority of the gaps lie between 2 and 5 eV, and some materials have a value of around 6 eV to more than 10 eV. First, we focus on the samples with experimental band gaps to evaluate the selected methods with reference to the experimental data. Then, the evaluation is extended to the whole data set by adapting the calculated $G_0W_0@PBEsol$ and ACBN0 band gaps as reference data.

METHODS

For each material in the data set, geometry optimizations were performed in the framework of KS DFT by using the all-electron full-potential numeric atom-centered orbital approach [39] implemented in the Fritz Haber Institute ab-initio materials simulations (FHI-aims) program package. Numerical tabulation of atomic orbitals significantly enhances the flexibility of the basis functions and thus remarkably improves the efficiency of the DFT calculations with this package. We used the GGA PBEsol functional [40] for obtaining the relaxed geometries. This functional is a revised parameterization of PBE for a more accurate calculation of surface and crystal properties and especially the lattice constants of solids. The basis set and numerical grids were defined by “tight” default integration grid settings. We employed convergence criteria of 10^{-4} eV, 10^{-7} eV, and 10^{-5} eV/Å for the sum of KS eigenvalues, the total energy, and the atomic forces, respectively. For sampling of the Brillouin zone, Γ -centered Monkhorst-Pack \mathbf{k} -point grids were used such that the smallest distance between grid points in reciprocal space became less than or equal 0.15. This \mathbf{k} -point sampling method resulted in a variable \mathbf{k} mesh for materials with different structures and lattice vectors. Localized basis functions in the FHI-aims package allow for a very efficient implementation of the hybrid functionals for crystalline systems [41]. Therefore, we used the FHI-aims package to calculate the electronic structure with the HSE06 functional. The HSE06 calculations were conducted with the tight setting and convergence criteria of 10^{-3} eV and 10^{-6} eV for the sum of KS eigenvalues and the total energy, respectively.

We used the Exciting package [42] for electronic-structure calculations with the $G_0W_0@PBEsol$ and $PBEsol-1/2$ schemes. This package uses the full-potential linearized augmented plane wave (FPLAPW) method [43, 44] to solve the Kohn-Sham single-particle equations. In the FPLAPW method, the crystal unit cell is divided into atomic spheres and interstitial regions. In the atomic spheres, atomic orbitals and spherical harmonics are used for the expansion of the KS wave functions, while in the interstitial area, plane wave basis functions are adapted. In the DFT-1/2 method, a half-electron is removed from anion atoms to simulate a hole excitation in the system, required for estimation of the QP self-energy effects. The corresponding self-energy potential should be trimmed with a CUT radius parameter to prevent spurious interaction between neighboring charged anions. The preferred CUT parameter is the one that maximizes the band gap of the system. Here, all ground-state calculations were performed using PBEsol functional. The size of \mathbf{k} - and \mathbf{q} -point sampling grids, the number of empty states, the number of frequencies, and also the values of basis set cut-off $R_{MT}|\mathbf{G} + \mathbf{k}|_{max}$ for all materials are presented in the supplementary information (SI). We also used the FPLAPW scheme for electronic-structure calculations using the mBJ functional, as it is implemented in the WIEN2K computer package [45, 46]. Similar computational parameters to those employed for the Exciting package were used for mBJ band-gap calculations in WIEN2K.

For DFT+ U calculations, we used the AFLOW π pack-

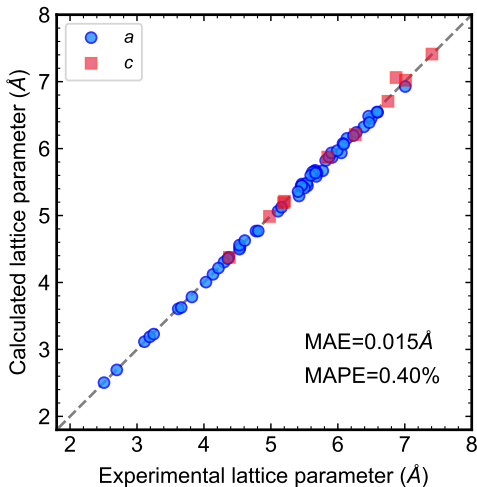


FIG. 2. Comparison between experimental and calculated lattice parameters within PBEsol. In the case of non-cubic structures, the vertical lattice parameter c is also displayed. The obtained mean absolute (percentage) error MA(P)E is also given in the figure.

age [47], which implements the ACBN0 approach using a projection on atomic orbitals [48–50] based on the output from Quantum ESPRESSO [51, 52] plane-wave code. Optimized norm-conserving (NC) Vanderbilt pseudopotentials [53] obtained from the PseudoDojo repository [54] were employed. For Li_2O , we used norm-conserving pseudopotential obtained from the Pslibrary [55]. In these calculations, a high plane-wave energy cutoff of 120 Ry together with a dense Monkhorst-Pack mesh was utilized to ensure good convergence of all quantities (see SI for the \mathbf{k} -point sampling for each material in the data set). The self-consistent Hubbard U values obtained within the ACBN0 scheme are presented in Table S6.

RESULTS AND DISCUSSIONS

Our data set contains 114 binary compounds with ten different crystal structures. After a broad literature survey, we separated 56 compounds from our data set, for which reliable experimental band gaps and lattice parameters are available in the literature. We note that only compounds with a non-zero PBEsol (or PBE) gap are included in the data set. PBEsol is found to be the most accurate GGA functional for obtaining the equilibrium parameter of crystals [7, 56, 57]. Hence, we used the PBEsol functional to calculate the relaxed geometry of the materials in our database. The obtained equilibrium parameters are compared with the experimental data in Fig. 2, and the corresponding relative errors are given in Supplementary Table S2. The references of the experimental data are also given in this table. As can be seen, there is an excellent agreement between the calculated and the measured lattice parameters, with a mean absolute percentage error of about 0.4%. Hence we used the PBEsol equilibrium parameters for

our band gap calculations within other desired schemes.

As others showed [59–61], zero-point vibrations [62] have a nontrivial contribution to the measured band gaps, even at extremely low temperatures. Therefore, a new theoretical scheme, zero-point renormalization (ZPR), is developed to correct the experimental band gaps for more accurate comparison with computational data. This scheme is out of the current paper’s scope. However, we applied the available ZPR corrections in the literature to our reference experimental band gaps (Fig. 1 and Supplementary Table S4). The band gaps calculated with different functionals are compared with the available experimental data in Fig. 3, while complementary details are presented in SI (Table S5). For more information, the direct gap of the samples with an indirect gap is also reported in this table. In these cases, the indirect band gaps were adapted for our following analysis.

The plots (Fig. 3) reveal that the band gaps obtained within the HSE06 and G_0W_0 @PBEsol methods, compared with PBEsol, are considerably improved, although they are still slightly underestimated with respect to the measured data. For better understanding, we performed a linear $y = ax + b$ least-square fit to these plots and presented the obtained slope a and intercept b parameters in Table I. The obtained slopes for HSE06 and G_0W_0 @PBEsol are 0.767 and 0.917 eV, respectively, while the corresponding intercepts are 0.276 and -0.165 eV. The smaller slope and high positive intercept of HSE06, which has enhanced after the inclusion of the large gap systems, evidence the weaker performance of this scheme for large band gap semiconductors compared with G_0W_0 @PBEsol. The obtained error distributions (Fig. 3 and Fig. S1) show that larger band gaps are better treated within G_0W_0 @PBEsol, while HSE06 exhibits slightly better performance in the smaller band gap materials. These figures show that in contrast to the HSE06 and G_0W_0 @PBEsol methods, which typically exhibit a small negative systematic error, ACBN0, PBEsol-1/2, and to a lower extent mBJ produce scattered band gaps around the experimental values. This behavior may be attributed to the case-dependent parameters in these computationally cheaper methods, which need proper optimization. In contrast, the fraction of the exact exchange in HSE06 is fixed based on first-principles considerations [63, 64], while the single range-separation parameter is fitted to improve band gap prediction accuracy.

To better evaluate the performance of the functionals in comparison with the reference (experimental) band gaps, we evaluate various error statistics [65], namely, Pearson’s correlation coefficient (r), Kendall’s rank correlation coefficient (τ) [66], the mean absolute error $\text{MAE} = \sum_i^n |y_i - y_{i,\text{exp}}|/n$, the mean error $\text{ME} = \sum_i^n (y_i - y_{i,\text{exp}})/n$, the error standard deviation $\text{STD} = (\sum_i^n (y_i - y_{i,\text{exp}} - \text{ME})^2/n)^{1/2}$, the median error MnE , the interquartile range IQR (difference between 3rd and 1st quartile), the median of the absolute deviations from the median MADM , the mean absolute percentage error $\text{MAPE} = 100 \times \sum_i^n |y_i - y_{i,\text{exp}}|/(ny_{i,\text{exp}})$, and the mean percentage error $\text{MPE} = 100 \times \sum_i^n (y_i - y_{i,\text{exp}})/(ny_{i,\text{exp}})$. The obtained error parameters are presented in Table I.

The inexpensive PBEsol-1/2, ACBN0, and mBJ schemes have small mean error values of -0.15, -0.19, and -0.36 eV,

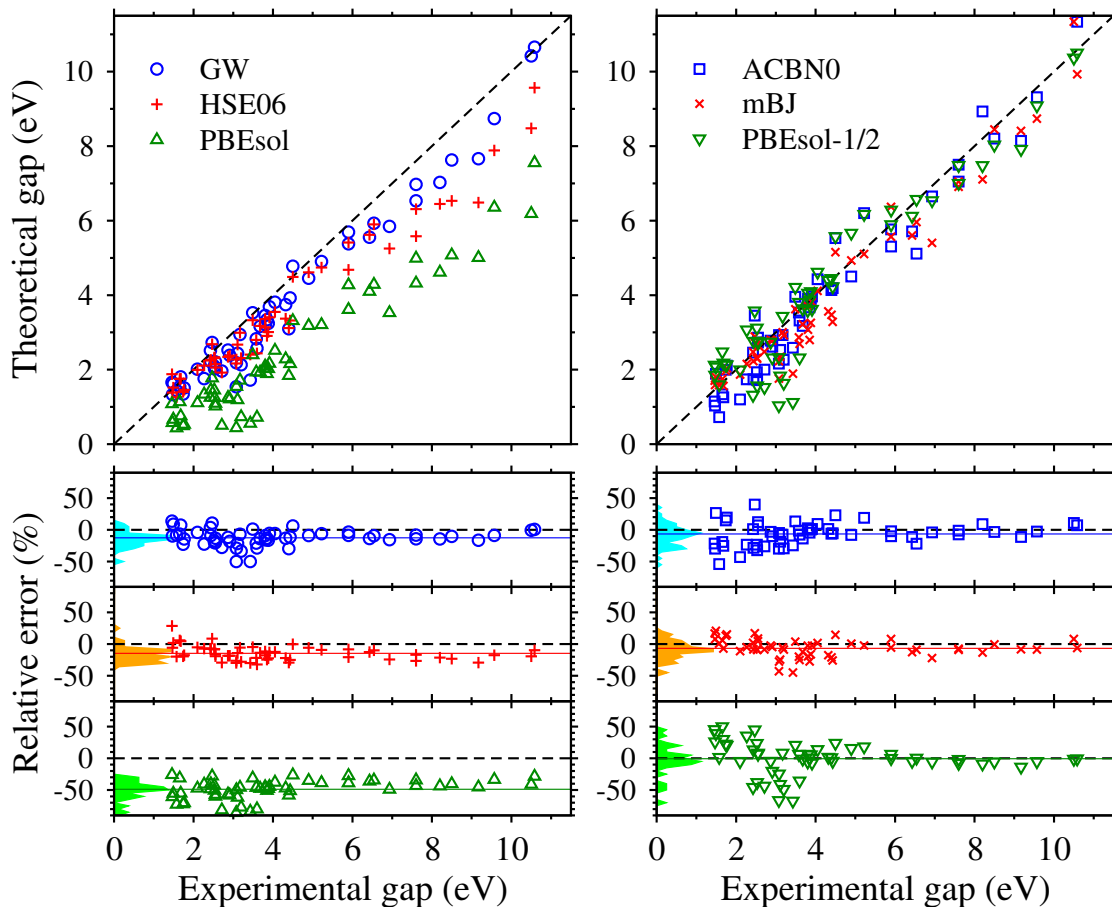


FIG. 3. Comparison of theoretical and experimental band gaps for 56 compounds in our data set. The dashed lines correspond to the coincidence of theory and experiment. The relative difference between the theoretical and experimental gaps is also calculated and plotted as a function of the experimental gap. In the relative error plots, the solid lines indicate the MPE values (Table I) and the shaded areas show the distribution histogram of the relative errors in arbitrary units.

while G_0W_0 @PBEsol and HSE06 give high ME values of about -0.53 and -0.75 eV, respectively. This fact does not indicate the higher accuracy of the cheaper methods; it rather demonstrates the mentioned unsystematic error behavior of these methods compared with the more systematic errors of HSE06 and G_0W_0 @PBEsol. The unsystematic error distributions are usually accompanied by significant error cancellation and thus lead to low mean error values. Therefore, MAE is more appropriate for comparing the accuracy of these methods. The ACBN0 and mBJ methods exhibit lower MAE values (0.48 and 0.52 eV) and thus are more accurate than PBEsol-1/2, HSE06, and G_0W_0 @PBEsol with MAE values above 0.57 eV. In terms of MAPE, mBJ exhibits the lowest error (12.1%), while ACBN0 and G_0W_0 @PBEsol show slightly larger errors. In addition to the classical statistical measures, we have used MnE, MADM, and IQR, which are less sensitive to outliers [65, 67]. The results show that PBEsol-1/2 and mBJ have the lowest MnE value of 0.01 and -0.22 eV, respectively, while G_0W_0 @PBEsol has the lowest IQR and MADM values.

Correlation coefficients are statistical parameters that evaluate the accuracy of the models in predicting the trend of the

target quantities compared with the reference data. In this regard, we calculated Pearson's and Kendall's rank correlations between theoretical and experimental band gaps and presented the results in Table I. G_0W_0 @PBEsol has the highest Pearson's correlation with the experiment, followed by HSE06 and then other methods. Considering Kendall's rank correlation, the mBJ, G_0W_0 @PBEsol, ACBN0, and HSE06 schemes give comparable values in the range of 0.83-0.87, whereas PBEsol-1/2 and PBEsol provide smaller values.

Among the 13 statistical parameters presented in Table I, we have highlighted ten more proper overall measures for a general comparative evaluation of the selected theoretical methods. The ME and MPE parameters are not used for this evaluation because of the involved error cancellation in these parameters. The median error MnE is also sensitive to the systematic or unsystematic error behavior of the methods and hence may not be useful for our comparative evaluation. Taking into account the highlighted parameters, one can conclude that G_0W_0 @PBEsol and ACBN0 provide the best performance for predicting the experimental band gap of semiconductors. G_0W_0 @PBEsol is the most (second) accurate method according to four (four) parameters, whereas

TABLE I. Statistical error measures of the calculated band gaps within different computational schemes, with respect to the experimental data (Exp.), G_0W_0 @PBEsol data (G_0W_0), and ACBN0 data. The experimental data cover 56 binary compounds, while theoretical G_0W_0 and ACBN0 data are calculated for the whole data set of 114 compounds. The highlighted blue and black numbers show the best and the second-best records within each parameter and reference, respectively, selected with a slight tolerance (0.01 eV or 0.1%).

Ref.		Pearson (%)	Kendall (%)	a	b (eV)	ME (eV)	MPE (%)	STD (eV)	MAE (eV)	MAPE (%)	MnE (eV)	IQR (eV)	MADM (eV)	MaxAE (eV)
Exp.	PBEsol	96.7	74.1	0.66	-0.49	-1.99	-48.8	1.07	1.99	48.8	-1.73	1.27	0.57	6.29
	PBEsol-1/2	95.9	73.2	0.90	0.27	-0.15	-0.6	0.80	0.60	18.3	0.01	0.90	0.44	2.31
	HSE06	98.4	86.5	0.77	0.28	-0.75	-14.7	0.76	0.78	16.4	-0.52	0.81	0.35	3.88
	mBJ	97.8	83.4	0.90	0.07	-0.36	-6.8	0.61	0.52	12.1	-0.22	0.81	0.42	2.58
	ACBN0	98.1	85.8	1.01	-0.22	-0.19	-6.5	0.57	0.48	14.3	-0.26	0.65	0.33	1.43
	G_0W_0	98.5	84.1	0.92	-0.16	-0.53	-12.5	0.50	0.57	14.4	-0.51	0.55	0.29	2.08
G_0W_0	PBEsol	98.0	83.2	0.72	-0.36	-1.30	-42.1	0.70	1.30	42.1	-1.25	0.65	0.34	4.24
	PBEsol-1/2	95.8	78.0	0.98	0.52	0.43	26.1	0.65	0.67	35.2	0.55	0.72	0.35	2.69
	ACBN0	97.3	83.1	1.07	0.07	0.30	12.4	0.58	0.53	23.0	0.33	0.77	0.37	1.99
	mBJ	98.1	86.5	0.98	0.29	0.23	12.7	0.44	0.35	15.8	0.17	0.36	0.17	2.13
	HSE06	99.3	89.3	0.84	0.44	-0.11	4.4	0.43	0.30	12.4	-0.04	0.43	0.23	1.95
	ACBN0	PBEsol	94.7	73.7	0.64	-0.26	-1.60	-44.3	1.04	1.60	44.3	-1.57	1.25	0.56
PBEsol-1/2		95.0	74.6	0.88	0.57	0.13	15.3	0.77	0.62	29.7	0.16	1.05	0.51	1.69
HSE06		96.4	81.2	0.74	0.54	-0.41	-1.3	0.81	0.69	22.6	-0.36	1.08	0.54	3.17
mBJ		97.2	82.5	0.89	0.35	-0.07	5.2	0.60	0.49	19.3	-0.05	0.94	0.47	1.83
G_0W_0		97.3	83.1	0.89	0.11	-0.30	-3.7	0.58	0.53	19.2	-0.33	0.77	0.37	1.99

ACBN0 is the best (second) scheme within three (six) statistical measures. The mBJ and HSE06 functionals take the next places when compared with the experimental data. mBJ gives the best MAPE and b parameters and the second-best MAE value, while HSE06 exhibits the highest Pearson and Kendall correlations. In fact, mBJ is more accurate than HSE06 in the reproduction of the measured band gaps, in agreement with recent publications [68, 69]. Taking into account the expensive computational cost of HSE06 and G_0W_0 @PBEsol, the above discussion indicates that ACBN0 and mBJ are clearly more efficient than HSE06 for band gap calculations. Moreover, ACBN0 is found to be a very good and reliable replacement instead of G_0W_0 @PBEsol for high-throughput screening of band gaps.

Based on the above analysis, in the rest of the paper, we choose G_0W_0 @PBEsol and ACBN0 as our first-principles reference methods and evaluate the performance of the other approaches in the whole data set of 114 binary materials. The calculated statistical measures compared with G_0W_0 @PBEsol and ACBN0 are separately given in Table I, and the corresponding radar plots and histograms are displayed in Fig. 4 and Figs. S2 and S3 (SI), respectively.

In comparison with the G_0W_0 @PBEsol reference data, HSE06 exhibits the best agreement with six first and one second records. The mBJ scheme takes second place with three first and five second records, and the ACBN0 takes third place with only one first and three second records. The weaker performance of ACBN0 in reproducing the G_0W_0 band gaps, compared with mBJ, looks strange because of the very similar performance of ACBN0 and G_0W_0 in reproducing the experimental band gaps. A more accurate inspection of the error histograms (Fig. 3) and ME values (Table I) indicates that, as it was mentioned before, mBJ lies between G_0W_0 and ACBN0

from the point of view of the underestimation of the experimental gap. As a result, mBJ is more successful than ACBN0 in reproducing the G_0W_0 @PBEsol band gaps.

On the other hand, adapting the ACBN0 band gaps as our reference data, we found that G_0W_0 @PBEsol and mBJ exhibit the best performances (Table I and Fig. 4). Although G_0W_0 has eight first records, mBJ has a slightly lower MAE and hence really competes with G_0W_0 in reproducing the ACBN0 band gaps. HSE06 take third place only with three second records. The point that seems strange is the fact that while HSE06 is the first and ACBN0 is the third successful method in producing the G_0W_0 band gaps (mentioned in the previous paragraph), in reproducing the ACBN0 band gaps, G_0W_0 is the most prosperous scheme. Again, we attribute this behavior to the rather systematic error behavior of G_0W_0 and HSE06 and the unsystematic error behavior of ACBN0. The obtained ME values indicate that the G_0W_0 band gaps are statistically distributed above the HSE06 and below the ACBN0 data, being closer to the HSE06 data. For example, compared with the experimental references, the ME value for HSE06, G_0W_0 , and ACBN0 are -0.75, -0.53, and -0.19 eV, respectively, which confirm the claimed order between these three schemes. The same arguments apply to theoretical references as well. As a result, compared with the G_0W_0 reference, HSE06 is more consistent than ACBN0, while in comparison with the ACBN0 data, the G_0W_0 scheme is more accurate than HSE06.

Finally, we calculate the Pearson coefficient to analyze the mutual correlations between the selected theoretical schemes and the experiment. These results may be useful to identify the best low-fidelity band gaps for machine learning modeling of the high-fidelity G_0W_0 @PBEsol band gaps. The obtained Pearson's correlation map for the considered approxi-

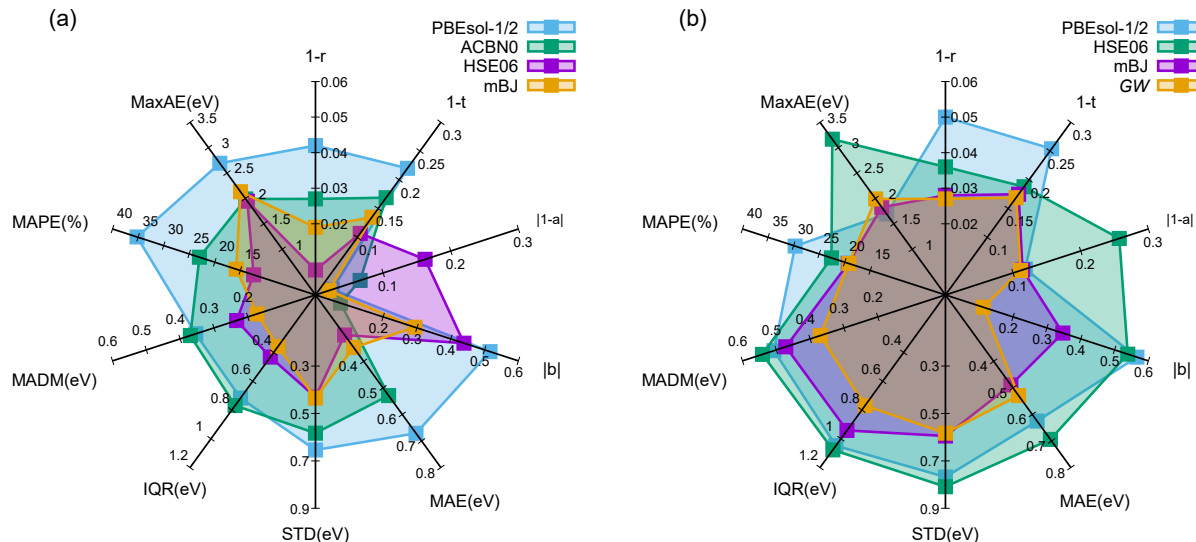


FIG. 4. Radar plots showing the ten more important statistical error quantities (Table I) calculated for 114 binary materials within different theoretical schemes with reference to the (a) G_0W_0 @PBEsol and (b) ACBN0 band gap data.

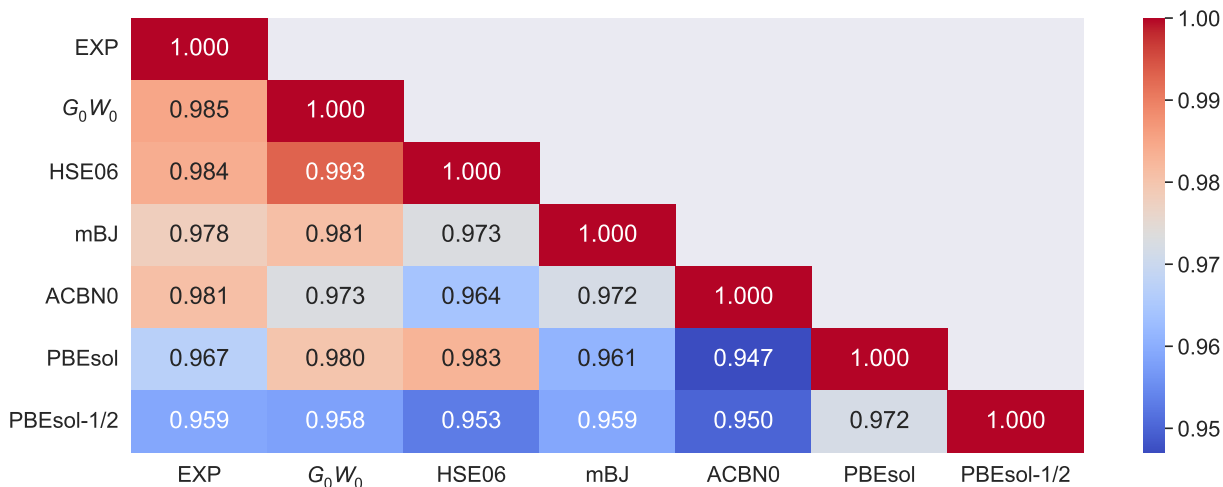


FIG. 5. Obtained Pearson's correlation heatmap among the selected theoretical schemes and experimental (Exp) data.

mations is presented in Fig. 5. It is clear that all theoretical methods correlate quite well (96% and more) with the experiment. Hence, all selected schemes, even conventional PBEsol, are expected to provide a reliable description of the band gap trends in different situations. Among the economic schemes, mBJ exhibits the highest correlation with the G_0W_0 @PBEsol method. Taking into account this fact along with the high agreement between the mBJ band gaps and the G_0W_0 ones, we conclude that the mBJ band gap is a very good descriptor for machine learning prediction of the quasiparticle G_0W_0 band gaps.

CONCLUSIONS

We have performed an extensive benchmark calculation within various exchange-correlation schemes, including G_0W_0 @PBEsol, hybrid HSE06, GGA PBEsol, meta-GGA mBJ, quasiparticle-corrected PBEsol-1/2, and pseudo-hybrid self-consistent ACBN0 functionals to evaluate their performance in predicting band gaps of semiconductors. We used a data set of 56 binary materials for evaluating the selected schemes with respect to the experiment, while in a broader group of 114 binary compounds, the G_0W_0 @PBEsol and ACBN0 schemes were adapted as a reference to assess other theoretical methods. Compared with the experiment, G_0W_0 @PBEsol outperforms overall all other functionals, although the mean absolute error (MAE) within

ACBN0 and mBJ (0.48 and 0.51 eV) are slightly better than $G_0W_0@PBEsol$ (0.57 eV). HSE06 shows the best correlations with the experiment, although its statistical error measures are less refined than ACBN0, especially for the larger band gap semiconductors. Overall, it is argued that ACBN0 is a promising alternative for the expensive G_0W_0 scheme for high-throughput scanning of the band gap of semiconductors and insulators.

In the group of 114 compounds, HSE06 shows the best agreement with the reference $G_0W_0@PBEsol$ data, with a very low MAE of about 0.30 eV and mBJ closely follow HSE06 in reproducing the reference band gaps. Despite its success in predicting the experimental data, the performance of ACBN0 in producing the G_0W_0 results is considerably less than mBJ. The reason is that the G_0W_0 and HSE06 band gaps are mainly below the experimental values, while the ACBN0

and $PBEsol-1/2$ values are scattered around the measured data, leading to the lowest mean errors of -0.19 and -0.15 eV, respectively. The mBJ functional exhibits a median behavior with a mean error of -0.36 eV, thus showing more agreement with G_0W_0 , compared with ACBN0. We conclude that the economic mBJ method helps produce cheap band gap descriptors for artificial intelligence modeling of the expensive $G_0W_0@PBEsol$ band gaps.

ACKNOWLEDGMENTS

This work was supported by RFBR-INSF grant number 20-53-56065.

-
- [1] W. Kohn and L. J. Sham, Self-consistent equations including exchange and correlation effects, *Phys. Rev.* **140**, A1133 (1965).
- [2] P. Hohenberg and W. Kohn, Inhomogeneous electron gas, *Phys. Rev.* **136**, B864 (1964).
- [3] J. P. Perdew, W. Yang, K. Burke, Z. Yang, E. K. U. Gross, M. Scheffler, G. E. Scuseria, T. M. Henderson, I. Y. Zhang, A. Ruzsinszky, H. Peng, J. Sun, E. Trushin, and A. Görling, Understanding band gaps of solids in generalized kohn-sham theory, *Proceedings of the National Academy of Sciences* **114**, 2801 (2017).
- [4] J. P. Perdew and A. Zunger, Self-interaction correction to density-functional approximations for many-electron systems, *Phys. Rev. B* **23**, 5048 (1981).
- [5] J. P. Perdew, K. Burke, and M. Ernzerhof, Generalized gradient approximation made simple, *Phys. Rev. Lett.* **77**, 3865 (1996).
- [6] J. P. Perdew and M. Levy, Physical content of the exact kohn-sham orbital energies: Band gaps and derivative discontinuities, *Phys. Rev. Lett.* **51**, 1884 (1983).
- [7] L. J. Sham and M. Schlüter, Density-functional theory of the energy gap, *Phys. Rev. Lett.* **51**, 1888 (1983).
- [8] J. P. Perdew, R. G. Parr, M. Levy, and J. L. Balduz, Density-functional theory for fractional particle number: Derivative discontinuities of the energy, *Phys. Rev. Lett.* **49**, 1691 (1982).
- [9] J. Heyd, G. E. Scuseria, and M. Ernzerhof, Hybrid functionals based on a screened coulomb potential, *The Journal of Chemical Physics* **118**, 8207 (2003).
- [10] J. Heyd, G. E. Scuseria, and M. Ernzerhof, Erratum: “hybrid functionals based on a screened coulomb potential” [j. chem. phys. 118, 8207 (2003)], *The Journal of Chemical Physics* **124**, 219906 (2006).
- [11] J. Sun, A. Ruzsinszky, and J. P. Perdew, Strongly constrained and appropriately normed semilocal density functional, *Phys. Rev. Lett.* **115**, 036402 (2015).
- [12] J. Sun, R. C. Remsing, Y. Zhang, Z. Sun, A. Ruzsinszky, H. Peng, Z. Yang, A. Paul, U. Waghmare, X. Wu, *et al.*, Accurate first-principles structures and energies of diversely bonded systems from an efficient density functional, *Nature chemistry* **8**, 831 (2016).
- [13] F. Della Sala, E. Fabiano, and L. A. Constantin, Kinetic-energy-density dependent semilocal exchange-correlation functionals, *International Journal of Quantum Chemistry* **116**, 1641 (2016).
- [14] A. I. Liechtenstein, V. I. Anisimov, and J. Zaanen, Density-functional theory and strong interactions: Orbital ordering in mott-hubbard insulators, *Phys. Rev. B* **52**, R5467 (1995).
- [15] V. I. Anisimov, F. Aryasetiawan, and A. I. Liechtenstein, First-principles calculations of the electronic structure and spectra of strongly correlated systems: the lda+u method, *Journal of Physics: Condensed Matter* **9**, 767 (1997).
- [16] L. G. Ferreira, M. Marques, and L. K. Teles, Approximation to density functional theory for the calculation of band gaps of semiconductors, *Phys. Rev. B* **78**, 125116 (2008).
- [17] L. G. Ferreira, M. Marques, and L. K. Teles, Slater half-occupation technique revisited: the lda-1/2 and gga-1/2 approaches for atomic ionization energies and band gaps in semiconductors, *AIP Advances* **1**, 032119 (2011).
- [18] K.-H. Xue, J.-H. Yuan, L. R. Fonseca, and X.-S. Miao, Improved lda-1/2 method for band structure calculations in covalent semiconductors, *Computational Materials Science* **153**, 493 (2018).
- [19] J. Doumont, F. Tran, and P. Blaha, Limitations of the dft-1/2 method for covalent semiconductors and transition-metal oxides, *Phys. Rev. B* **99**, 115101 (2019).
- [20] A. Georges and G. Kotliar, Hubbard model in infinite dimensions, *Phys. Rev. B* **45**, 6479 (1992).
- [21] A. Georges, G. Kotliar, W. Krauth, and M. J. Rozenberg, Dynamical mean-field theory of strongly correlated fermion systems and the limit of infinite dimensions, *Rev. Mod. Phys.* **68**, 13 (1996).
- [22] G. Kotliar, S. Y. Savrasov, K. Haule, V. S. Oudovenko, O. Parcollet, and C. A. Marianetti, Electronic structure calculations with dynamical mean-field theory, *Rev. Mod. Phys.* **78**, 865 (2006).
- [23] F. Aryasetiawan and O. Gunnarsson, The gw method, *Reports on Progress in Physics* **61**, 237 (1998).
- [24] F. Fuchs, J. Furthmüller, F. Bechstedt, M. Shishkin, and G. Kresse, Quasiparticle band structure based on a generalized kohn-sham scheme, *Phys. Rev. B* **76**, 115109 (2007).
- [25] M. Shishkin and G. Kresse, Self-consistent gw calculations for semiconductors and insulators, *Phys. Rev. B* **75**, 235102 (2007).
- [4] J. Heyd, J. E. Peralta, G. E. Scuseria, and R. L. Martin, Energy band gaps and lattice parameters evaluated with the heyd-scuseria-ernzerhof screened hybrid functional, *The Journal of Chemical Physics* **123**, 174101 (2005).

- [27] P. Rinke, A. Qteish, J. Neugebauer, C. Freysoldt, and M. Scheffler, Combining gw calculations with exact-exchange density-functional theory: an analysis of valence-band photoemission for compound semiconductors, *New Journal of Physics* **7**, 126 (2005).
- [28] M. Springer and F. Aryasetiawan, Frequency-dependent screened interaction in ni within the random-phase approximation, *Phys. Rev. B* **57**, 4364 (1998).
- [29] M. Cococcioni and S. de Gironcoli, Linear response approach to the calculation of the effective interaction parameters in the LDA + U method, *Phys. Rev. B* **71**, 035105 (2005).
- [30] F. Tran and P. Blaha, Accurate band gaps of semiconductors and insulators with a semilocal exchange-correlation potential, *Phys. Rev. Lett.* **102**, 226401 (2009).
- [31] P. Borlido, T. Aull, A. W. Huran, F. Tran, M. A. L. Marques, and S. Botti, Large-scale benchmark of exchange-correlation functionals for the determination of electronic band gaps of solids, *Journal of Chemical Theory and Computation* **15**, 5069 (2019).
- [32] F. Tran, J. Doumont, L. Kalantari, A. W. Huran, M. A. L. Marques, and P. Blaha, Semilocal exchange-correlation potentials for solid-state calculations: Current status and future directions, *Journal of Applied Physics* **126**, 110902 (2019).
- [33] J. C. Slater, Statistical exchange-correlation in the self-consistent field (Academic Press, 1972) pp. 1–92.
- [34] J. C. Slater and K. H. Johnson, Self-consistent-field $x\alpha$ cluster method for polyatomic molecules and solids, *Phys. Rev. B* **5**, 844 (1972).
- [35] L. G. Ferreira, R. R. Pelá, L. K. Teles, M. Marques, M. Ribeiro Jr., and J. Furthmüller, The lda-1/2 technique: Recent developments, *AIP Conference Proceedings* **1566**, 27 (2013).
- [36] R. R. Pela, A. Gulans, and C. Draxl, The lda-1/2 method implemented in the exciting code, *Computer Physics Communications* **220**, 263 (2017).
- [37] R. Rodrigues Pela, U. Werner, D. Nabok, and C. Draxl, Probing the lda-1/2 method as a starting point for G_0W_0 calculations, *Phys. Rev. B* **94**, 235141 (2016).
- [38] M. De Jong, W. Chen, T. Angsten, A. Jain, R. Notestine, A. Gamst, M. Sluiter, C. Krishna Ande, S. Van Der Zwaag, J. J. Plata, *et al.*, Charting the complete elastic properties of inorganic crystalline compounds, *Scientific data* **2**, 1 (2015).
- [39] V. Blum, R. Gehrke, F. Hanke, P. Havu, V. Havu, X. Ren, K. Reuter, and M. Scheffler, Ab initio molecular simulations with numeric atom-centered orbitals, *Computer Physics Communications* **180**, 2175 (2009).
- [40] J. P. Perdew, A. Ruzsinszky, G. I. Csonka, O. A. Vydrov, G. E. Scuseria, L. A. Constantin, X. Zhou, and K. Burke, Restoring the density-gradient expansion for exchange in solids and surfaces, *Phys. Rev. Lett.* **100**, 136406 (2008).
- [41] S. V. Levchenko, X. Ren, J. Wierfink, R. Johanni, P. Rinke, V. Blum, and M. Scheffler, Hybrid functionals for large periodic systems in an all-electron, numeric atom-centered basis framework, *Computer Physics Communications* **192**, 60 (2015).
- [42] A. Gulans, S. Kontur, C. Meisenbichler, D. Nabok, P. Pavone, S. Rigamonti, S. Sagsmeister, U. Werner, and C. Draxl, exciting: a full-potential all-electron package implementing density-functional theory and many-body perturbation theory, *Journal of Physics: Condensed Matter* **26**, 363202 (2014).
- [43] D. J. Singh and L. Nordstrom, *Planewaves, Pseudopotentials, and the LAPW method* (Springer New York, NY, 2006).
- [44] F. Karsai, F. Tran, and P. Blaha, On the importance of local orbitals using second energy derivatives for d and f electrons, *Computer Physics Communications* **220**, 230 (2017).
- [45] P. Blaha, K. Schwarz, G. K. H. Madsen, D. Kvasnicka, J. Luitz, R. Laskowski, F. Tran, and L. D. Marks, *WIEN2k, An Augmented Plane Wave + Local Orbitals Program for Calculating Crystal Properties* (Karlheinz Schwarz, Techn. Universitat Wien, Austria, 2018).
- [46] P. Blaha, K. Schwarz, F. Tran, R. Laskowski, G. K. H. Madsen, and L. D. Marks, Wien2k: An apw+lo program for calculating the properties of solids, *The Journal of Chemical Physics* **152**, 074101 (2020).
- [47] A. R. Supka, T. E. Lyons, L. Liyanage, P. D’Amico, R. A. R. A. Orabi, S. Mahatara, P. Gopal, C. Toher, D. Ceresoli, A. Calzolari, S. Curtarolo, M. B. Nardelli, and M. Fornari, Aflow π : A minimalist approach to high-throughput ab initio calculations including the generation of tight-binding hamiltonians, *Computational Materials Science* **136**, 76 (2017).
- [48] L. A. Agapito, A. Ferretti, A. Calzolari, S. Curtarolo, and M. Buongiorno Nardelli, Effective and accurate representation of extended bloch states on finite hilbert spaces, *Phys. Rev. B* **88**, 165127 (2013).
- [49] L. A. Agapito, S. Ismail-Beigi, S. Curtarolo, M. Fornari, and M. B. Nardelli, Accurate tight-binding hamiltonian matrices from ab initio calculations: Minimal basis sets, *Phys. Rev. B* **93**, 035104 (2016).
- [50] L. A. Agapito, M. Fornari, D. Ceresoli, A. Ferretti, S. Curtarolo, and M. B. Nardelli, Accurate tight-binding hamiltonians for two-dimensional and layered materials, *Phys. Rev. B* **93**, 125137 (2016).
- [51] P. Giannozzi, S. Baroni, N. Bonini, M. Calandra, R. Car, C. Cavazzoni, D. Ceresoli, G. L. Chiarotti, M. Cococcioni, I. Dabo, A. D. Corso, S. de Gironcoli, S. Fabris, G. Fratesi, R. Gebauer, U. Gerstmann, C. Gougoussis, A. Kokalj, M. Lazzeri, L. Martin-Samos, N. Marzari, F. Mauri, R. Mazzarello, S. Paolini, A. Pasquarello, L. Paulatto, C. Sbraccia, S. Scandolo, G. Sclauzero, A. P. Seitsonen, A. Smogunov, P. Umari, and R. M. Wentzcovitch, Quantum espresso: a modular and open-source software project for quantum simulations of materials, *Journal of Physics: Condensed Matter* **21**, 395502 (2009).
- [52] P. Giannozzi, O. Andreussi, T. Brumme, O. Bunau, M. B. Nardelli, M. Calandra, R. Car, C. Cavazzoni, D. Ceresoli, M. Cococcioni, N. Colonna, I. Carnimeo, A. D. Corso, S. de Gironcoli, P. Delugas, R. A. DiStasio, A. Ferretti, A. Floris, G. Fratesi, G. Fugallo, R. Gebauer, U. Gerstmann, F. Giustino, T. Gorni, J. Jia, M. Kawamura, H.-Y. Ko, A. Kokalj, E. Küçükbenli, M. Lazzeri, M. Marsili, N. Marzari, F. Mauri, N. L. Nguyen, H.-V. Nguyen, A. O. de-la Roza, L. Paulatto, S. Poncé, D. Rocca, R. Sabatini, B. Santra, M. Schlipf, A. P. Seitsonen, A. Smogunov, I. Timrov, T. Thonhauser, P. Umari, N. Vast, X. Wu, and S. Baroni, Advanced capabilities for materials modelling with quantum espresso, *Journal of Physics: Condensed Matter* **29**, 465901 (2017).
- [53] D. R. Hamann, Optimized norm-conserving vanderbilt pseudopotentials, *Phys. Rev. B* **88**, 085117 (2013).
- [54] M. van Setten, M. Giantomassi, E. Bousquet, M. Verstraete, D. Hamann, X. Gonze, and G.-M. Rignanese, The pseudodojo: Training and grading a 85 element optimized norm-conserving pseudopotential table, *Computer Physics Communications* **226**, 39 (2018).
- [55] A. D. Corso, Pseudopotentials periodic table: From h to pu, *Computational Materials Science* **95**, 337 (2014).
- [56] L. Schimka, J. Harl, and G. Kresse, Improved hybrid functional for solids: The hsesol functional, *The Journal of Chemical Physics* **134**, 024116 (2011).

- [57] G.-X. Zhang, A. M. Reilly, A. Tkatchenko, and M. Scheffler, Performance of various density-functional approximations for cohesive properties of 64 bulk solids, *New Journal of Physics* **20**, 063020 (2018).
- [7] P. Haas, F. Tran, and P. Blaha, Calculation of the lattice constant of solids with semilocal functionals, *Phys. Rev. B* **79**, 085104 (2009).
- [59] F. Karsai, M. Engel, E. Flage-Larsen, and G. Kresse, Electron-phonon coupling in semiconductors within the gw approximation, *New Journal of Physics* **20**, 123008 (2018).
- [60] A. Miglio, V. Brousseau-Couture, E. Godbout, G. Antonius, Y.-H. Chan, S. G. Louie, M. Côté, M. Giantomassi, and X. Gonze, Predominance of non-adiabatic effects in zero-point renormalization of the electronic band gap, *npj Computational Materials* **6**, 1 (2020).
- [61] M. Engel, H. Miranda, L. Chaput, A. Togo, C. Verdi, M. Marsman, and G. Kresse, Zero-point renormalization of the band gap of semiconductors and insulators using the projector augmented wave method, *Phys. Rev. B* **106**, 094316 (2022).
- [62] G. D. Mahan, *Many-particle physics* (Springer New York, NY, 2000).
- [63] D. Langreth and J. Perdew, The exchange-correlation energy of a metallic surface, *Solid State Communications* **17**, 1425 (1975).
- [64] J. P. Perdew, M. Ernzerhof, and K. Burke, Rationale for mixing exact exchange with density functional approximations, *The Journal of Chemical Physics* **105**, 9982 (1996).
- [65] B. Civalleri, D. Presti, R. Dovesi, and A. Savin, On choosing the best density functional approximation, *Chemical Modelling: Applications and Theory Volume 9* **9**, 168 (2012).
- [66] M. G. Kendall, A new measure of rank correlation, *Biometrika* **30**, 81 (1938).
- [67] P. Kaliraj and T. Devi, *Big Data Applications in Industry 4.0 (1st ed.)* (Auerbach Publications, 2022).
- [68] T. c. v. Rauch, M. A. L. Marques, and S. Botti, Accurate electronic band gaps of two-dimensional materials from the local modified becke-johnson potential, *Phys. Rev. B* **101**, 245163 (2020).
- [69] F. Tran, J. Doumont, L. Kalantari, P. Blaha, T. Rauch, P. Borlido, S. Botti, M. A. L. Marques, A. Patra, S. Jana, and P. Samal, Bandgap of two-dimensional materials: Thorough assessment of modern exchange-correlation functionals, *The Journal of Chemical Physics* **155**, 104103 (2021).

SUPPLEMENTARY INFORMATION

Table S1 shows the most important parameters used for G_0W_0 @PBESol calculations in the EXCITING package. These parameters include the \mathbf{k} -point sampling, the \mathbf{q} -point sampling, the number of empty states, the number of frequencies, and the values of RKmtmax. The experimental lattice parameters of 56 structures, compared with calculated values, are illustrated in Table S2. In Table S3, we present the \mathbf{k} -point sampling used in Quantum-Espresso code for ACBN0 calculations, as described in the main text. The obtained ACBN0 band gaps and Hubbard U parameters of binary materials are tabulated in Tables S5 and S6, respectively. In Table S5, the list of all binary compounds with their calculated band gaps in the functionals considered in this benchmark study is presented. This table also contains the Materials Project identification number (MP id), the number of space groups, the experimental band gap if it is available, and also the type of PBESol band gap. Table S4 gives the collected available zero-phonon renormalization (ZPR) values in the literature.

TABLE S1. Computational parameters used for G_0W_0 @PBESol calculations. From left to right: Wavevector sampling for the electronic states; wavevector sampling for the phonon states; the number of empty states; the number of frequencies; the basis set cut-off $R_{MT}|\mathbf{G} + \mathbf{k}|_{max}$.

	\mathbf{k} -point sampling	\mathbf{q} -point sampling	# of empty states	frequency	rgkmax		\mathbf{k} -point sampling	\mathbf{q} -point sampling	# of empty states	frequency	rgkmax
AgBr-216	16 × 16 × 16	8 × 8 × 8	16	32	7.5	GaP-186	14 × 14 × 7	8 × 8 × 4	18	32	7.0
AgBr-225	16 × 16 × 16	8 × 8 × 8	12	32	7.5	GaP-216	16 × 16 × 16	6 × 6 × 6	16	32	8.0
AgCl-221	16 × 16 × 16	8 × 8 × 8	16	32	7.0	GeC-186	14 × 14 × 7	8 × 8 × 4	14	18	7.0
AgCl-225	16 × 16 × 16	8 × 8 × 8	16	32	7.5	GeC-216	12 × 12 × 12	8 × 8 × 8	16	32	7.0
AgI-216	14 × 14 × 14	8 × 8 × 8	18	32	7.5	InP-216	16 × 16 × 16	8 × 8 × 8	16	32	7.0
AgI-225	16 × 16 × 16	8 × 8 × 8	18	32	8.0	K2O-225	16 × 16 × 16	8 × 8 × 8	14	32	7.5
AlAs-186	14 × 14 × 8	8 × 8 × 4	18	32	7.0	K2S-225	15 × 15 × 15	6 × 6 × 6	18	32	7.5
AlAs-216	12 × 12 × 12	8 × 8 × 8	14	32	7.0	K2Se-225	16 × 16 × 16	8 × 8 × 8	18	32	7.0
AlN-186	16 × 16 × 9	8 × 8 × 4	18	32	6.5	KBr-225	12 × 12 × 12	8 × 8 × 8	20	32	7.5
AlN-216	12 × 12 × 12	8 × 8 × 8	16	32	7.0	KCl-225	12 × 12 × 12	8 × 8 × 8	20	32	7.0
AlN-225	14 × 14 × 14	8 × 8 × 8	16	32	7.0	Li2O-225	15 × 15 × 15	8 × 8 × 8	18	32	7.5
AlP-186	12 × 12 × 8	8 × 8 × 4	18	32	7.0	Li2S-225	14 × 14 × 14	8 × 8 × 8	18	32	7.0
AlP-216	14 × 14 × 14	8 × 8 × 8	16	32	7.0	Li2Se-225	16 × 16 × 16	8 × 8 × 8	18	32	7.5
AlSb-216	16 × 16 × 16	6 × 6 × 6	16	32	7.0	LiBr-225	12 × 12 × 12	8 × 8 × 8	20	32	7.5
BaCl2-225	16 × 16 × 16	6 × 6 × 6	18	32	7.8	LiCl-225	12 × 12 × 12	8 × 8 × 8	20	32	7.0
BaO-129	10 × 10 × 12	6 × 6 × 7	20	32	7.0	LiF-225	12 × 12 × 12	8 × 8 × 8	20	32	7.0
BaO-225	14 × 14 × 14	8 × 8 × 8	18	32	7.5	Mg2Si-225	14 × 14 × 14	8 × 8 × 8	18	32	7.0
Bas-186	13 × 13 × 7	8 × 8 × 4	18	32	6.0	MgO-187	14 × 14 × 13	8 × 8 × 8	16	32	7.0
Bas-216	14 × 14 × 14	8 × 8 × 8	14	32	6.0	MgO2-166	14 × 14 × 14	8 × 8 × 8	20	32	7.5
BaS-225	16 × 16 × 16	8 × 8 × 8	18	32	7.5	MgO-225	13 × 13 × 13	8 × 8 × 8	16	32	7.5
BaSe-221	16 × 16 × 16	8 × 8 × 8	18	32	8.0	MgS-186	14 × 14 × 7	8 × 8 × 4	18	32	7.0
BaSe-225	11 × 11 × 11	8 × 8 × 8	18	32	8.0	MgS-216	14 × 14 × 14	8 × 8 × 8	18	32	7.0
BaTe-221	18 × 18 × 18	8 × 8 × 8	18	32	8.0	MgS-225	14 × 14 × 14	8 × 8 × 8	20	32	7.0
BaTe-225	18 × 18 × 18	8 × 8 × 8	18	32	8.0	MgSe-186	16 × 16 × 8	8 × 8 × 4	18	16	7.0
Be2C-225	12 × 12 × 12	8 × 8 × 8	16	32	7.0	MgSe-216	18 × 18 × 18	8 × 8 × 8	20	32	8.0
BeO-186	15 × 15 × 8	8 × 8 × 4	20	32	6.5	MgSe-225	16 × 16 × 16	8 × 8 × 8	16	32	8.0
BeS-216	14 × 14 × 14	8 × 8 × 8	16	32	7.0	MgTe-186	13 × 13 × 7	7 × 7 × 4	20	32	7.5
BeSe-194	12 × 12 × 6	8 × 8 × 4	16	32	7.0	Na2O-225	16 × 16 × 16	6 × 6 × 6	16	32	7.5
BeSe-216	12 × 12 × 12	8 × 8 × 8	16	32	7.0	Na2S-225	14 × 14 × 14	8 × 8 × 8	16	32	7.5
BN-186	16 × 16 × 8	8 × 8 × 4	18	32	7.0	Na2Se-225	16 × 16 × 16	8 × 8 × 8	18	32	7.5
BN-194	17 × 17 × 4	8 × 8 × 2	14	32	7.0	NaCl-225	12 × 12 × 12	8 × 8 × 8	20	32	7.5
BN-216	14 × 14 × 14	8 × 8 × 8	14	32	7.0	NaF-225	12 × 12 × 12	8 × 8 × 8	20	32	7.5
BP-186	14 × 14 × 7	8 × 8 × 4	18	32	7.0	NaF-225	14 × 14 × 14	8 × 8 × 8	20	32	8.0
BP-216	12 × 12 × 12	6 × 6 × 6	10	32	6.0	PbSe-225	14 × 14 × 14	8 × 8 × 8	20	32	7.5
BSb-216	16 × 16 × 16	8 × 8 × 8	16	32	7.0	PbTe-225	14 × 14 × 14	7 × 7 × 7	20	32	7.5
Ca2Ge-225	16 × 16 × 16	8 × 8 × 8	16	32	7.5	ScN-216	14 × 14 × 14	6 × 6 × 6	14	32	7.0
CaO-225	14 × 14 × 14	8 × 8 × 8	16	32	7.0	ScP-216	14 × 14 × 14	8 × 8 × 8	18	32	7.0
CaS-225	14 × 14 × 14	8 × 8 × 8	16	32	6.0	SiC-186	14 × 14 × 7	8 × 8 × 4	16	32	7.0
CaSe-216	16 × 16 × 16	6 × 6 × 6	16	32	7.0	SiC-216	14 × 14 × 14	8 × 8 × 8	16	32	7.0
CaSe-225	15 × 15 × 15	8 × 8 × 8	14	32	7.5	SiGe-216	15 × 15 × 15	6 × 6 × 6	16	32	7.0
CdS-186	14 × 14 × 7	8 × 8 × 4	16	16	7.0	SiO2-225	14 × 14 × 14	8 × 8 × 8	16	32	7.0
CdS-216	12 × 12 × 12	8 × 8 × 8	16	32	7.0	SiSn-216	16 × 16 × 16	8 × 8 × 8	16	32	7.5
CdSe-186	15 × 15 × 8	8 × 8 × 4	18	16	7.5	SnC-216	16 × 16 × 16	8 × 8 × 8	16	32	7.0
CdSe-216	14 × 14 × 14	8 × 8 × 8	16	32	8.0	SrO-225	14 × 14 × 14	8 × 8 × 8	14	32	7.0
CdTe-216	12 × 12 × 12	8 × 8 × 8	16	32	7.8	SrS-225	14 × 14 × 14	8 × 8 × 8	16	32	7.0
CuBr-119	12 × 12 × 14	8 × 8 × 6	16	32	7.0	SrSe-225	14 × 14 × 14	8 × 8 × 8	16	32	7.5
CuBr-194	16 × 16 × 8	8 × 8 × 4	18	32	7.0	TiO2-225	16 × 16 × 16	8 × 8 × 8	18	32	7.0
CuBr-216	16 × 16 × 16	8 × 8 × 8	16	32	7.5	ZnO-186	14 × 14 × 7	8 × 8 × 4	16	32	7.5
CuCl-216	16 × 16 × 16	8 × 8 × 8	16	32	7.0	ZnO-216	14 × 14 × 14	8 × 8 × 8	20	32	7.0
CuCl-225	14 × 14 × 14	8 × 8 × 8	16	32	7.5	ZnO-225	14 × 14 × 14	8 × 8 × 8	18	32	7.5
CuI-186	16 × 16 × 8	8 × 8 × 4	16	32	7.5	ZnS-186	14 × 14 × 7	8 × 8 × 4	16	32	7.0
CuI-216	16 × 16 × 16	8 × 8 × 8	16	32	8.0	ZnS-216	14 × 14 × 14	8 × 8 × 8	20	32	7.0
GaAs-216	16 × 16 × 16	8 × 8 × 8	14	32	8.0	ZnSe-186	16 × 16 × 8	8 × 8 × 4	14	32	7.5
GaN-186	14 × 14 × 8	8 × 8 × 4	14	32	7.0	ZnSe-216	18 × 18 × 18	8 × 8 × 8	16	32	7.5
GaN-194	16 × 16 × 6	8 × 8 × 3	18	16	7.0	ZnTe-216	12 × 12 × 12	8 × 8 × 8	16	32	8.0
GaN-216	12 × 12 × 12	6 × 6 × 6	10	32	7.0	ZrO2-225	14 × 14 × 14	8 × 8 × 8	16	32	7.0
GaN-225	14 × 14 × 14	8 × 8 × 8	18	32	7.0	ZrS2-164	14 × 14 × 7	8 × 8 × 4	16	32	7.0

TABLE S2. Theoretical and experimental lattice constants (\AA) for the set of 56 binary compounds. Theoretical lattice parameters are calculated by PBEsol functional.

	exp.a	exp.c	conventional.a	c	relative_error_conv.a	relative_error.c	ref
AgBr-225	5.775		5.669		1.839		[1]
AgCl-225	5.546		5.443		1.854		[2]
AgI-216	6.499		6.451		0.745		[1]
AlAs-216	5.661		5.675		0.244		[1]
AlN-186	3.111	4.979	3.115	4.986	0.139	0.152	[1]
AlN-216	4.370		4.377		0.171		[3]
AlP-216	5.464		5.470		0.125		[1]
AlSb-216	6.136		6.153		0.279		[1]
BAs-216	4.777		4.768		0.192		[1]
BN-194	2.507	6.870	2.504	7.061	0.127	2.787	[1]
BN-216	3.616		3.606		0.274		[1]
BP-216	4.538		4.521		0.391		[1]
BaO-225	5.536		5.486		0.907		[1]
BaS-225	6.389		6.325		1.003		[4]
BaSe-225	6.595		6.541		0.815		[4]
BaTe-225	7.007		6.927		1.148		[4]
BeO-186	2.698	4.380	2.694	4.375	0.135	0.122	[1]
CaO-225	4.811		4.769		0.866		[1]
CaS-225	5.689		5.634		0.966		[4]
CaSe-225	5.916		5.868		0.803		[4]
CdS-186	4.135	6.749	4.121	6.706	0.323	0.632	[1]
CdS-216	5.818		5.821		0.059		[4]
CdSe-186	4.300	7.011	4.304	7.021	0.100	0.147	[1]
CdSe-216	6.077		6.077		0.004		[1]
CdTe-216	6.460		6.484		0.364		[1]
CuBr-216	5.677		5.584		1.640		[1]
CuCl-216	5.420		5.292		2.373		[1]
CuI-216	6.052		5.936		1.923		[1]
GaAs-216	5.654		5.660		0.107		[1]
GaN-186	3.190	5.189	3.187	5.192	0.085	0.053	[1]
GaN-216	4.531		4.498		0.732		[1]
GaP-216	5.451		5.439		0.222		[1]
InP-216	5.869		5.875		0.109		[1]
KBr-225	6.585		6.547		0.581		[5]
KCl-225	6.277		6.242		0.559		[5]
LiBr-225	5.501		5.409		1.681		[6]
LiCl-225	5.106		5.064		0.822		[7]
LiF-225	4.030		4.006		0.607		[8]
MgO-225	4.216		4.215		0.019		[1]
MgS-216	5.622		5.651		0.524		[4]
MgSe-216	5.904		5.936		0.539		[1]
MgSe-225	5.460		5.449		0.201		[1]
MgTe-186	4.530	7.406	4.558	7.412	0.603	0.085	[1]
NaCl-225	5.595		5.601		0.100		[7]
NaF-225	4.609		4.626		0.368		[7]
NaI-225	6.470		6.388		1.260		[9]
SiC-216	4.358		4.357		0.027		[4]
SrO-225	5.159		5.123		0.690		[1]
SrS-225	5.990		5.969		0.358		[4]
SrSe-225	6.234		6.194		0.643		[4]
ZnO-186	3.249	5.204	3.229	5.213	0.624	0.177	[1]
ZnS-186	3.820	6.260	3.784	6.209	0.953	0.809	[1]
ZnS-216	5.405		5.357		0.886		[1]
ZnSe-216	5.667		5.634		0.588		[1]
ZnTe-216	6.088		6.064		0.391		[1]
ZrS2-164	3.660	5.850	3.626	5.873	0.927	0.394	[10]

TABLE S3. **k**-point sampling used for ACBN0 calculations

	k -point sampling		k -point sampling
AgBr-216	12 × 12 × 12	GaP-186	13 × 13 × 7
AgBr-225	13 × 13 × 13	GaP-216	14 × 14 × 14
AgCl-221	13 × 13 × 13	GeC-186	16 × 16 × 8
AgCl-225	14 × 14 × 14	GeC-216	16 × 16 × 16
AgI-216	12 × 12 × 12	InP-216	13 × 13 × 13
AgI-225	13 × 13 × 13	K2O-225	12 × 12 × 12
AlAs-186	13 × 13 × 7	K2S-225	10 × 10 × 10
AlAs-216	13 × 13 × 13	K2Se-225	10 × 10 × 10
AlN-186	16 × 16 × 9	KBr-225	12 × 12 × 12
AlN-216	17 × 17 × 17	KCl-225	12 × 12 × 12
AlN-225	18 × 18 × 18	Li2O-225	16 × 16 × 16
AlP-186	13 × 13 × 7	Li2S-225	13 × 13 × 13
AlP-216	14 × 14 × 14	Li2Se-225	13 × 13 × 13
AlSb-216	12 × 12 × 12	LiBr-225	14 × 14 × 14
BaCl2-225	11 × 11 × 11	LiCl-225	15 × 15 × 15
BaO-129	10 × 10 × 12	LiF-225	19 × 19 × 19
BaO-225	14 × 14 × 14	Mg2Si-225	12 × 12 × 12
Bas-186	15 × 15 × 8	MgO-187	17 × 17 × 16
Bas-216	16 × 16 × 16	MgO2-166	16 × 16 × 16
BaS-225	12 × 12 × 12	MgO-225	18 × 18 × 18
BaSe-221	11 × 11 × 11	MgS-186	13 × 13 × 7
BaSe-225	12 × 12 × 12	MgS-216	13 × 13 × 13
BaTe-221	11 × 11 × 11	MgS-225	12 × 12 × 12
BaTe-225	11 × 11 × 11	MgSe-186	13 × 13 × 7
Be2C-225	17 × 17 × 17	MgSe-216	13 × 13 × 13
BeO-186	18 × 18 × 10	MgSe-225	14 × 14 × 14
BeS-216	15 × 15 × 15	MgTe-186	11 × 11 × 6
BeSe-194	14 × 14 × 8	Na2O-225	14 × 14 × 14
BeSe-216	15 × 15 × 15	Na2S-225	12 × 12 × 12
BN-186	20 × 20 × 10	Na2Se-225	11 × 11 × 11
BN-194	20 × 20 × 6	NaCl-225	13 × 13 × 13
BN-216	21 × 21 × 21	NaF-225	16 × 16 × 16
BP-186	16 × 16 × 8	NaI-225	12 × 12 × 12
BP-216	17 × 17 × 17	PbSe-225	12 × 12 × 12
BSb-216	14 × 14 × 14	PbTe-225	12 × 12 × 12
Ca2Ge-225	11 × 11 × 11	ScN-216	15 × 15 × 15
CaO-225	16 × 16 × 16	ScP-216	15 × 15 × 15
CaS-225	13 × 13 × 13	SiC-186	17 × 17 × 9
CaSe-216	12 × 12 × 12	SiC-216	17 × 17 × 17
CaSe-225	13 × 13 × 13	SiGe-216	14 × 14 × 14
CdS-186	13 × 13 × 7	SiO2-225	16 × 16 × 16
CdS-216	13 × 13 × 13	SiSn-216	13 × 13 × 13
CdSe-186	12 × 12 × 6	SnC-216	15 × 15 × 15
CdSe-216	12 × 12 × 12	SrO-225	15 × 15 × 15
CdTe-216	12 × 12 × 12	SrS-225	13 × 13 × 13
CuBr-119	13 × 13 × 16	SrSe-225	12 × 12 × 12
CuBr-194	13 × 13 × 8	TiO2-225	16 × 16 × 16
CuBr-216	13 × 13 × 13	ZnO-186	16 × 16 × 9
CuCl-216	14 × 14 × 14	ZnO-216	16 × 16 × 16
CuCl-225	15 × 15 × 15	ZnO-225	18 × 18 × 18
CuI-186	13 × 13 × 7	ZnS-186	13 × 13 × 7
CuI-216	13 × 13 × 13	ZnS-216	14 × 14 × 14
GaAs-216	13 × 13 × 13	ZnSe-186	13 × 13 × 7
GaN-186	16 × 16 × 9	ZnSe-216	13 × 13 × 13
GaN-194	17 × 17 × 6	ZnTe-216	12 × 12 × 12
GaN-216	17 × 17 × 17	ZrO2-225	15 × 15 × 15
GaN-225	18 × 18 × 18	ZrS2-164	14 × 14 × 8

TABLE S4. Available values of ZPR for materials used in this study. The values are obtained from references [11] and [12].

	ZPR (eV)
AlAs-216	0.039
AlN-186	0.239
AlP-216	0.023
AlSb-216	0.039
BN-216	0.340
CdS-186	0.068
CdSe-186	0.034
CdTe-216	0.017
CuBr-216	0.005
CuCl-216	0.031
CuI-216	-0.009
GaAs-216	0.054
GaN-186	0.173
GaP-216	0.085
InP-216	0.048
LiCl-225	0.170
LiF-225	1.150
MgO-225	0.530
NaCl-225	0.170
SiC-216	0.110
ZnO-186	0.156
ZnS-216	0.080
ZnSe-216	0.047
ZnTe-216	0.033

TABLE S5: List of the binary materials considered in the present benchmark study. From left to right: Material; Materials Project ID; available experimental band gaps; band gaps calculated with different approaches.

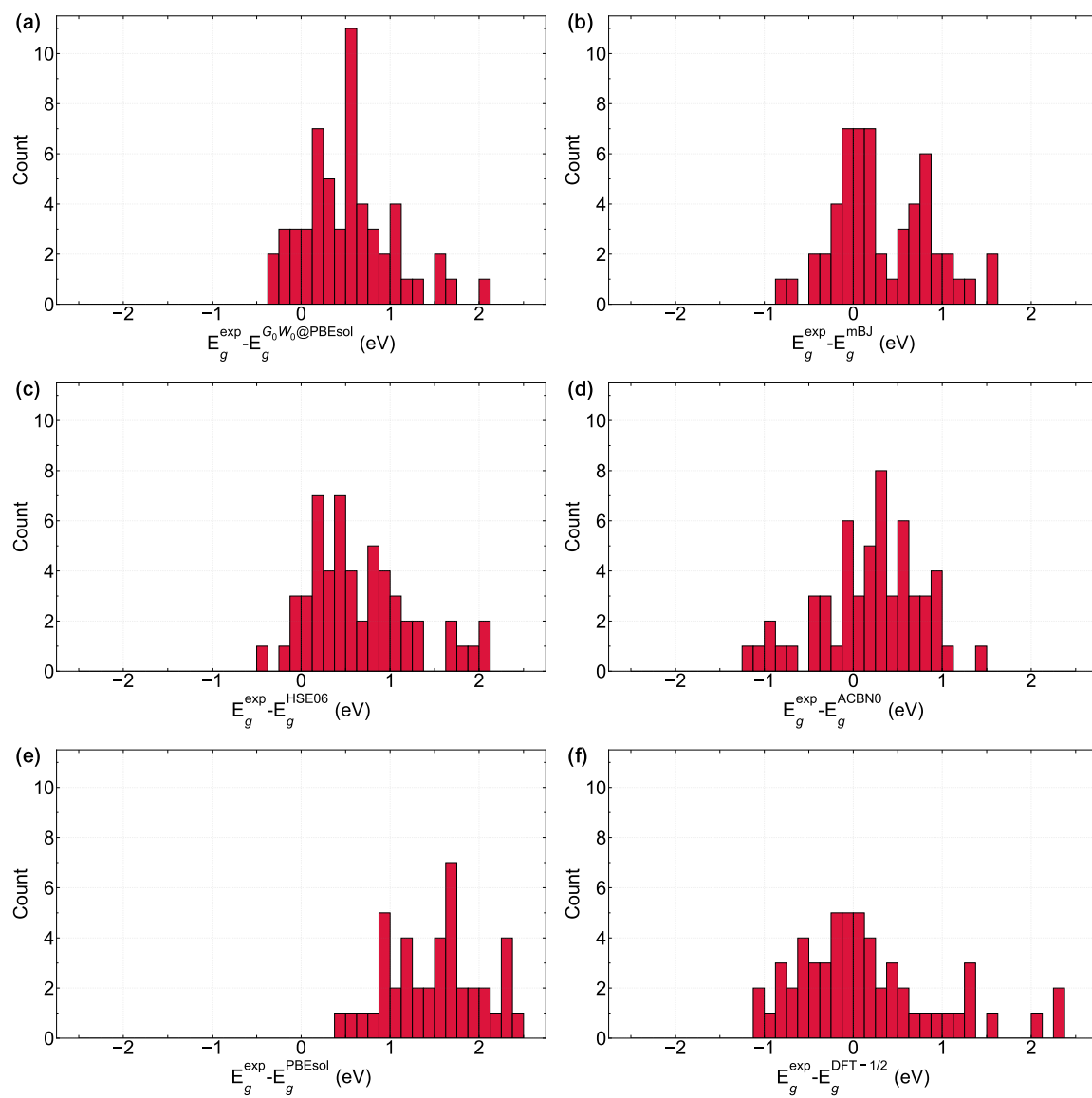
Material	MP id	SG	Expt.	PBEsol	type	mBJ	DFT-1/2	HSE06	ACBN0	G_0W_0	DIR	INDIR
AgBr	mp-866291	216		0.889	direct	2.891	1.942	2.248	2.390	2.199	2.199	
AgBr	mp-23231	225	2.712[1]	0.502	indir	2.480	1.526	1.920	2.002	1.963	3.824	1.963
AgCl	mp-1060502	221		0.453	indir	2.685	1.403	1.961	1.959	1.721	3.574	1.721
AgCl	mp-22922	225	3.200[1]	0.731	indir	2.924	1.637	2.310	2.267	2.130	4.691	2.130
AgI	mp-22925	216	2.910[1]	1.212	direct	2.775	2.318	2.376	2.615	2.382	2.382	
AgI	mp-22919	225		0.386	indir	1.731	1.427	1.514	1.713	1.383	3.764	1.383
AlAs	mp-8881	186		1.618	indir	2.408	3.149	2.384	2.036	2.138	2.419	2.138
AlAs	mp-2172	216	2.229[1]	1.339	indir	2.155	3.069	2.107	1.740	1.759	2.826	1.759
AlN	mp-661	186	6.190[1]	4.099	direct	5.603	6.121	5.621	5.710	5.554	5.554	
AlN	mp-1700	216	4.900[3]	3.181	indir	4.932	5.667	4.612	4.502	4.455	5.550	4.455
AlN	mp-1330	225		4.524	indir	6.164	6.801	6.010	5.820	6.081	7.276	6.081
AlP	mp-8880	186		1.823	indir	2.636	3.330	2.680	2.308	2.540	3.201	2.540
AlP	mp-1550	216	2.500[1]	1.449	indir	2.316	3.121	2.313	1.930	2.092	4.041	2.092
AlSb	mp-2624	216	1.615[1]	1.136	indir	1.750	2.480	1.751	1.339	1.541	2.935	1.541
BA	mp-984718	186		1.052	indir	1.651	2.117	1.822	1.109	1.523	2.922	1.523
BA	mp-10044	216	1.460[1]	1.081	indir	1.703	2.122	1.879	1.145	1.660	4.127	1.660
BN	mp-2653	186		5.042	indir	6.946	7.404	6.599	5.710	7.000	10.585	7.000
BN	mp-984	194	5.900[1]	4.275	indir	6.371	6.287	5.413	5.304	5.692	6.399	5.692
BN	mp-1639	216	6.200[1]	4.285	indir	5.961	6.574	5.898	5.113	5.930	11.087	5.930
BP	mp-1008559	186		0.909	indir	1.777	1.989	1.704	0.929	1.655	3.554	1.655
BP	mp-1479	216	2.100[1]	1.109	indir	1.867	1.998	1.994	1.198	2.013	4.406	2.013
BSb	mp-997618	216		0.657	indir	1.089	1.440	1.284	0.736	0.934	3.405	0.934
BaCl2	mp-568662	225		5.529	direct	7.388	6.847	6.919	8.186	7.607	7.796	7.607
BaO	mp-7487	129		3.610	indir	4.644	4.766	4.985	5.860	5.213	5.277	5.213
BaO	mp-1342	225	4.4[1]	1.839	indir	3.472	4.451	3.116	4.137	3.097	3.097	
BaS	mp-1500	225	3.880[4]	2.023	indir	3.256	4.096	3.010	3.899	3.243	4.774	3.243
BaSe	mp-10680	221		1.156	indir	2.022	3.075	1.970	2.552	2.021	2.215	2.021
BaSe	mp-1253	225	3.580[4]	1.932	indir	2.865	3.810	2.797	3.535	2.828	4.183	2.828
BaTe	mp-2600	221		0.640	indir	1.336	2.393	1.341	1.804	1.176	1.543	1.176
BaTe	mp-1000	225	3.080[4]	1.546	indir	2.230	2.326	2.272	2.928	2.186	3.949	2.186
Be2C	mp-1569	225		1.064	indir	1.864	2.932	1.966	2.014	1.748	5.216	1.748
BeO	mp-2542	186	10.585[1]	7.553	direct	9.931	10.504	9.568	11.338	10.658	10.658	
BeS	mp-422	216		2.905	indir	4.159	4.865	4.061	4.666	4.197	7.323	4.197
BeSe	mp-1008524	194		0.435	indir	0.952	2.069	1.056	1.675	0.842	3.148	0.842
BeSe	mp-1541	216		2.459	indir	3.501	4.421	3.446	3.986	3.404	5.614	3.404
Ca2Ge	mp-1009755	225		0.505	direct	0.956	1.757	1.043	0.883	0.836	1.988	0.836
CaO	mp-2605	225	6.931[1]	3.527	indir	5.404	6.540	5.250	6.650	5.847	6.383	5.847
CaS	mp-1672	225	4.430[13]	2.158	indir	3.284	4.227	3.320	4.189	3.926	6.428	3.926
CaSe	mp-1008223	216		3.125	indir	4.740	5.301	4.051	5.221	4.412	4.486	4.412
CaSe	mp-1415	225	3.850[13]	1.891	indir	2.797	3.874	2.906	3.673	3.342	4.506	3.342
CdS	mp-672	186	2.482[1]	1.095	direct	2.772	2.762	2.145	2.858	2.209	2.209	
CdS	mp-2469	216	2.550[4]	1.018	direct	2.664	2.720	2.060	2.729	2.034	2.034	
CdSe	mp-1070	186	1.732[1]	0.528	direct	2.036	2.132	1.455	2.107	1.511	1.511	
CdSe	mp-2691	216	1.740[1]	0.489	direct	1.967	2.130	1.402	1.997	1.346	1.346	
CdTe	mp-406	216	1.475[1]	0.665	direct	1.802	2.075	1.519	1.890	1.623	1.623	
CuBr	mp-32880	119		0.441	direct	1.733	0.990	2.117	2.181	1.523	1.523	
CuBr	mp-23227	194		0.410	direct	1.485	0.807	2.083	2.066	2.223	2.223	
CuBr	mp-22913	216	3.073[1]	0.438	direct	1.760	1.034	2.165	2.163	1.542	1.542	
CuCl	mp-22914	216	3.399[1]	0.557	direct	1.891	1.122	2.404	2.588	1.720	1.720	
CuCl	mp-571386	225		0.422	indir	1.848	0.853	2.423	2.516	1.593	3.346	1.593
CuI	mp-569346	186		1.233	direct	2.402	1.878	2.711	2.591	2.678	2.678	
CuI	mp-22895	216	3.118[1]	1.190	direct	2.346	1.833	2.671	2.532	2.437	2.437	
GaAs	mp-2534	216	1.519[1]	0.432	direct	1.584	1.598	1.263	0.723	1.443	1.443	
GaN	mp-804	186	3.503[1]	1.927	direct	3.219	3.636	3.173	3.174	3.164	3.164	
GaN	mp-1007824	194		1.319	indir	2.682	3.207	2.357	2.696	2.635	5.469	2.635
GaN	mp-830	216	3.170[1]	1.716	direct	3.003	3.435	2.988	2.930	2.945	2.945	
GaN	mp-2853	225		0.545	indir	2.179	2.626	1.747	1.527	1.768	3.847	1.768
GaP	mp-8882	186		1.296	direct	2.194	2.434	2.161	1.606	2.045	2.190	2.045
GaP	mp-2490	216	2.350[1]	1.455	indir	2.228	2.764	2.261	1.745	2.214	3.346	2.214
GeC	mp-1184550	186		2.268	indir	3.227	3.868	3.331	2.608	3.028	3.948	3.028
GeC	mp-1002164	216		1.517	indir	2.371	3.286	2.511	1.883	2.090	4.387	2.090
InP	mp-20351	216	1.424[1]	0.577	direct	1.587	1.856	1.384	1.035	1.330	1.330	
K2O	mp-971	225		1.856	indir	5.179	4.692	3.159	5.038	3.047	3.617	3.047
K2S	mp-1022	225		2.333	indir	5.203	4.610	3.319	4.524	3.722	3.933	3.722
K2Se	mp-8426	225		2.098	indir	4.514	4.212	2.990	4.080	3.322	3.458	3.322
KBr	mp-23251	225	7.600[14]	4.320	direct	7.047	7.003	5.582	7.049	6.531	6.531	
KCl	mp-23193	225	8.500[14]	5.076	direct	8.449	8.033	6.531	8.204	7.627	7.627	
Li2O	mp-1960	225		5.053	indir	7.832	8.056	6.561	7.006	6.962	7.450	6.962
Li2S	mp-1153	225		3.189	indir	4.766	5.391	4.289	5.296	4.668	5.727	4.668
Li2Se	mp-2286	225		2.802	indir	4.122	4.926	3.757	4.677	3.952	4.688	3.952
LiBr	mp-23259	225	7.600[15]	4.989	indir	6.910	7.485	6.310	7.502	6.972	6.972	
LiCl	mp-22905	225	9.400[15]	6.355	indir	8.737	9.085	7.883	9.317	8.739	8.739	
LiF	mp-1138	225	14.200[16]	9.057	indir	12.774	13.082	11.468	14.383	13.270	13.270	
Mg2Si	mp-1367	225		0.124	indir	0.552	1.453	0.614	0.910	0.336	2.338	0.336

Table S5 (Continued)

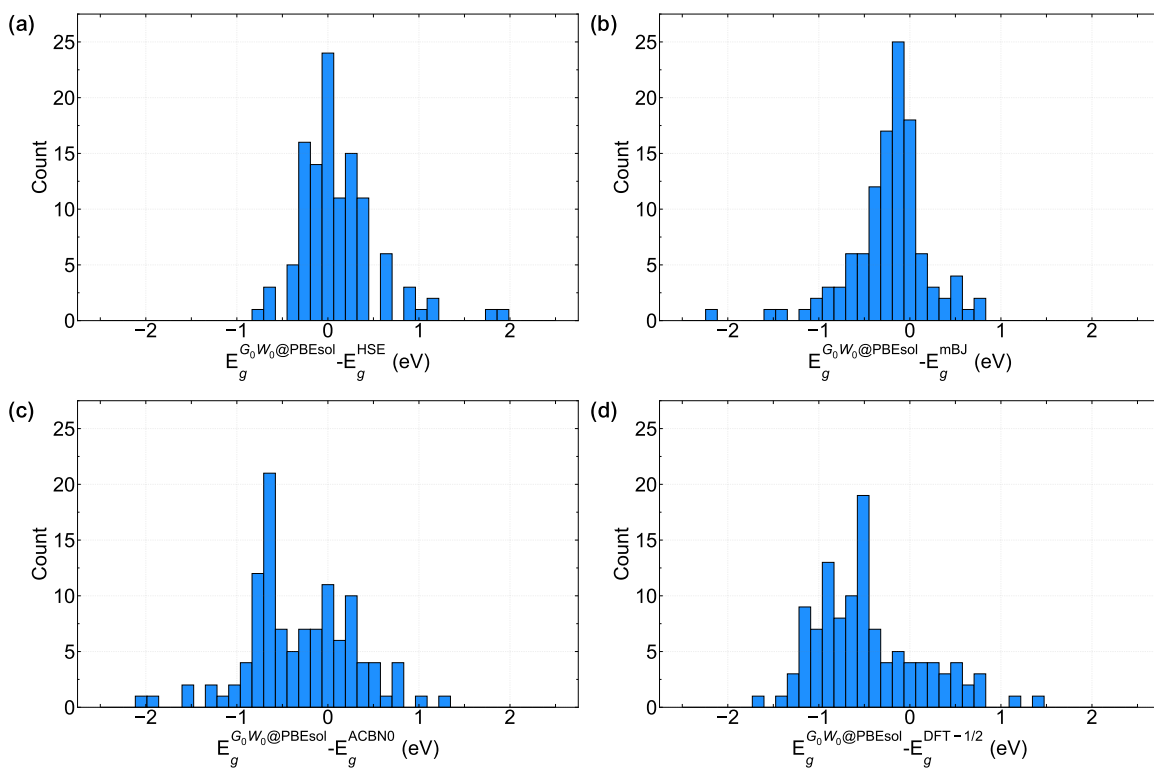
MgO	mp-1009129	187		3.138	indir	5.776	6.092	4.845	6.638	5.111	5.573	5.111
MgO	mp-1265	225	7.672[1]	4.614	direct	7.107	7.481	6.449	8.933	7.028	7.028	
MgO ₂	mp-1180271	166		2.473	direct	5.195	2.919	4.761	4.586	5.613	5.613	
MgS	mp-1185942	186		3.299	direct	5.149	5.459	4.450	5.554	4.722	4.722	
MgS	mp-13032	216	4.500[1]	3.311	direct	5.153	5.574	4.487	5.530	4.776	4.776	
MgS	mp-1315	225		2.727	indir	4.095	4.567	3.859	4.744	4.131	5.090	4.131
MgSe	mp-1018040	186		2.515	direct	4.157	4.649	3.574	4.476	3.813	3.813	
MgSe	mp-13031	216	4.050[1]	2.513	direct	4.116	4.618	3.551	4.427	3.809	3.809	
MgSe	mp-10760	225	2.470[4]	1.776	indir	2.891	3.579	2.683	3.452	2.729	3.712	2.729
MgTe	mp-1039	186	3.490[1]	2.398	direct	3.623	4.213	3.326	3.954	3.528	3.528	
Na ₂ O	mp-2352	225		1.977	indir	5.150	4.917	3.385	5.284	3.724	3.735	3.724
Na ₂ S	mp-648	225		2.425	direct	4.911	4.759	3.473	4.543	3.835	3.835	
Na ₂ Se	mp-1266	225		1.991	direct	4.098	4.181	2.933	3.869	3.236	3.236	
NaCl	mp-22862	225	9.000[14]	5.006	direct	8.410	7.916	6.485	8.140	7.662	7.662	
NaF	mp-682	225	10.500[14]	6.189	direct	11.342	10.367	8.478	11.645	10.424	10.424	
NaI	mp-23268	225	5.900[14]	3.610	direct	5.568	5.894	4.681	5.766	5.378	5.378	
PbSe	mp-2201	225		0.170	direct	0.777	1.346	0.609	0.696	0.169	0.169	
PbTe	mp-19717	225		0.641	direct	1.058	1.621	1.050	1.148	1.055	1.055	
ScN	mp-1009750	216		2.352	indir	3.710	4.136	3.612	3.358	3.375	5.660	3.375
ScP	mp-1009746	216		1.505	indir	2.153	2.836	2.406	2.197	2.330	4.784	2.330
SiC	mp-7140	186		2.160	indir	3.307	2.473	3.272	2.610	2.917	6.174	2.917
SiC	mp-8062	216	2.420[4]	1.250	indir	2.293	1.567	2.330	1.716	2.019	7.236	2.019
SiGe	mp-1219182	216		0.471	indir	1.123	1.511	1.139	0.489	0.997	3.138	0.997
SiO ₂	mp-10064	225		1.902	direct	4.044	4.645	3.576	3.655	3.483	3.483	
SiSn	mp-1009813	216		0.467	indir	1.053	0.970	1.080	0.495	0.791	1.401	0.791
SnC	mp-1009820	216		0.786	direct	1.395	1.885	1.634	1.296	1.319	1.319	
SrO	mp-2472	225	5.220[1]	3.206	indir	5.103	6.171	4.742	6.201	4.902	5.468	4.902
SrS	mp-1087	225	4.320[13]	2.286	indir	3.563	4.399	3.370	4.374	3.746	4.936	3.746
SrSe	mp-2758	225	3.810[13]	2.034	indir	3.073	4.057	3.130	3.906	3.213	4.122	3.213
TiO ₂	mp-1008677	225		1.075	indir	2.356	2.790	2.591	1.944	2.523	3.533	2.523
ZnO	mp-2133	186	3.441[1]	0.719	direct	2.694	2.320	2.437	3.318	2.571	2.571	
ZnO	mp-1986	216		0.614	direct	2.570	2.192	2.331	3.191	2.164	2.164	
ZnO	mp-2229	225		0.890	indir	2.929	2.420	2.687	3.579	2.631	3.623	2.631
ZnS	mp-560588	186	3.910[1]	2.166	direct	3.811	3.622	3.403	3.966	3.689	3.689	
ZnS	mp-10695	216	3.723[1]	2.094	direct	3.707	3.593	3.360	3.823	3.454	3.454	
ZnSe	mp-380	186		1.286	direct	2.852	2.812	2.383	2.886	2.705	2.705	
ZnSe	mp-1190	216	2.822[1]	1.248	direct	2.802	2.741	2.343	2.779	2.526	2.526	
ZnTe	mp-2176	216	2.394[1]	1.254	direct	2.474	1.317	2.247	2.457	2.516	2.516	
ZrO ₂	mp-1565	225		3.322	indir	4.699	5.848	5.028	5.078	5.188	5.418	5.188
ZrS ₂	mp-1186	164	1.680[10]	0.754	indir	1.562	2.182	1.755	1.256	1.806	2.782	1.806

TABLE S6. Converged values of U_{eff} (in eV) obtained from ACBN0 calculations.

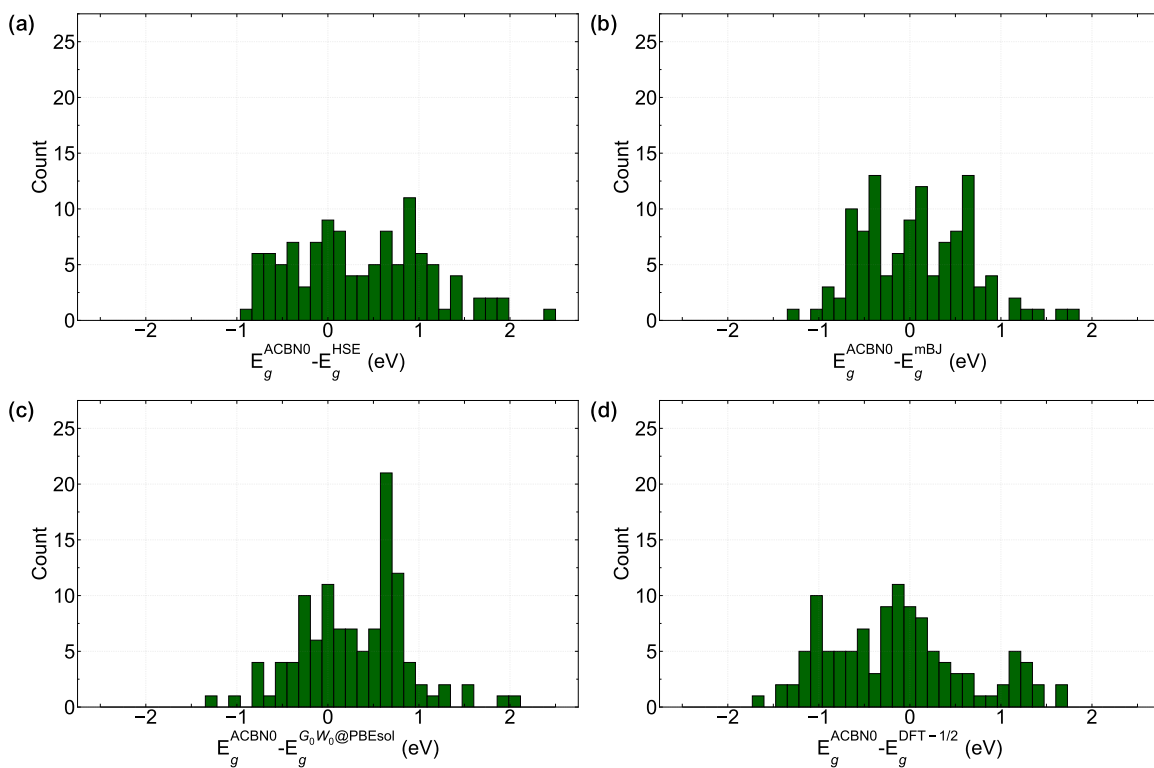
	U1	U2		U1	U2
BN-216	U_B = 0.24	U_N = 3.63	AgCl-221	U_Ag = 8.45	U_Cl = 3.46
BN-194	U_B = 0.16	U_N = 3.88	AgI-225	U_Ag = 9.27	U_I = 3.3
BP-216	U_B = 0.71	U_P = 0.92	AlAs-186	U_Al = 0.09	U_As = 2.01
BAAs-216	U_As = 0.85	U_B = 0.64	AlN-225	U_Al = 0.11	U_N = 4.93
AlN-186	U_Al = 0.05	U_N = 5.26	AlP-186	U_Al = 0.08	U_P = 2.27
AlP-216	U_Al = 0.08	U_P = 2.1	BaCl2-225	U_Ba = 0.0	U_Cl = 7.27
AlAs-216	U_Al = 0.09	U_As = 1.85	BaO-129	U_Ba = 0.16	U_O = 9.54
AlSb-216	U_Al = 0.12	U_Sb = 1.29	BAAs-186	U_As = 0.89	U_B = 0.75
GaN-186	U_Ga = 18.76	U_N = 4.31	BaSe-221	U_Ba = 0.02	U_Se = 5.83
GaN-216	U_Ga = 18.75	U_N = 4.02	BaTe-221	U_Ba = 0.01	U_Te = 5.13
GaP-216	U_Ga = 19.68	U_P = 1.66	Be2C-225	U_Be = 0.62	U_C = 4.38
GaAs-216	U_As = 1.45	U_Ga = 19.73	BeS-216	U_Be = 0.03	U_S = 6.41
InP-216	U_In = 15.69	U_P = 1.81	BeSe-194	U_Be = 0.05	U_Se = 6.36
BeO-186	U_Be = 0.02	U_O = 11.11	BeSe-216	U_Be = 0.04	U_Se = 5.87
MgO-225	U_Mg = 0.1	U_O = 10.75	BN-186	U_B = 0.24	U_N = 3.78
MgS-216	U_Mg = 0.03	U_S = 6.23	BP-186	U_B = 0.78	U_P = 0.95
MgSe-216	U_Mg = 0.04	U_Se = 5.58	BSb-216	U_B = 0.74	U_Sb = 0.56
CaO-225	U_Ca = 0.3	U_O = 10.58	Ca2Ge-225	U_Ca = 0.33	U_Ge = 1.57
SrO-225	U_O = 10.13	U_Sr = 0.35	CaSe-216	U_Ca = 0.01	U_Se = 5.89
BaO-225	U_Ba = 0.23	U_O = 9.42	CuBr-119	U_Br = 1.94	U_Cu = 9.13
ZnO-186	U_O = 7.06	U_Zn = 12.84	CuBr-194	U_Br = 2.2	U_Cu = 9.3
ZnS-216	U_S = 5.3	U_Zn = 13.95	CuCl-225	U_Cl = 2.04	U_Cu = 9.34
ZnS-186	U_S = 5.53	U_Zn = 13.87	Cu-186	U_Cu = 9.35	U_I = 2.13
ZnSe-216	U_Se = 5.0	U_Zn = 15.27	GaN-194	U_Ga = 18.67	U_N = 4.35
ZnTe-216	U_Te = 4.4	U_Zn = 17.53	GaN-225	U_Ga = 18.99	U_N = 4.19
CdS-186	U_Cd = 11.93	U_S = 5.46	GaP-186	U_Ga = 19.68	U_P = 1.8
CdSe-216	U_Cd = 12.51	U_Se = 4.92	GeC-186	U_C = 2.22	U_Ge = 0.24
CdSe-186	U_Cd = 12.54	U_Se = 5.08	GeC-216	U_C = 2.0	U_Ge = 0.23
CdTe-216	U_Cd = 13.95	U_Te = 4.3	K2O-225	U_K = 0.53	U_O = 10.25
CuCl-216	U_Cl = 2.04	U_Cu = 9.33	K2S-225	U_K = 0.11	U_S = 5.8
CuBr-216	U_Br = 1.88	U_Cu = 9.1	K2Se-225	U_K = 0.08	U_Se = 5.16
CuI-216	U_Cu = 9.4	U_I = 2.04	Li2O-225	U_Li = 0.63	U_O = 7.09
AgBr-225	U_Ag = 8.41	U_Br = 3.04	Li2S-225	U_Li = 0.17	U_S = 5.97
AgI-216	U_Ag = 9.23	U_I = 3.24	Li2Se-225	U_Li = 0.09	U_Se = 5.43
SiC-216	U_C = 2.52	U_Si = 0.19	Mg2Si-225	U_Mg = 0.31	U_Si = 3.55
CdS-216	U_Cd = 11.96	U_S = 5.34	MgO-187	U_Mg = 0.08	U_O = 10.66
MgSe-225	U_Mg = 0.03	U_Se = 5.8	MgO2-166	U_Mg = 0.01	U_O = 8.95
BaS-225	U_Ba = 0.04	U_S = 6.12	MgS-186	U_Mg = 0.03	U_S = 6.36
BaSe-225	U_Ba = 0.03	U_Se = 5.63	MgS-225	U_Mg = 0.03	U_S = 6.54
BaTe-225	U_Ba = 0.02	U_Te = 4.98	MgSe-186	U_Mg = 0.03	U_Se = 5.71
KCl-225	U_Cl = 7.31	U_K = 0.01	Na2O-225	U_Na = 1.05	U_O = 9.63
LiF-225	U_F = 12.98	U_Li = 0.09	Na2S-225	U_Na = 0.1	U_S = 5.68
NaCl-225	U_Cl = 7.53	U_Na = 0.01	Na2Se-225	U_Na = 0.07	U_Se = 5.06
NaI-225	U_I = 5.54	U_Na = 0.0	PbSe-225	U_Pb = 0.07	U_Se = 2.87
AgCl-225	U_Ag = 7.56	U_Cl = 2.68	PbTe-225	U_Pb = 0.1	U_Te = 2.36
KBr-225	U_Br = 6.45	U_K = 0.0	ScN-216	U_N = 4.88	U_Sc = 0.15
NaF-225	U_F = 12.76	U_Na = 0.04	ScP-216	U_P = 2.86	U_Sc = 0.19
CaS-225	U_Ca = 0.02	U_S = 6.63	SiC-186	U_C = 2.76	U_Si = 0.18
CaSe-225	U_Ca = 0.01	U_Se = 6.07	SiGe-216	U_Ge = 0.59	U_Si = 0.49
SrS-225	U_S = 6.44	U_Sr = 0.03	SiO2-225	U_O = 8.76	U_Si = 0.02
SrSe-225	U_Se = 5.89	U_Sr = 0.02	SiSn-216	U_Si = 0.61	U_Sn = 0.36
ZrS2-164	U_S = 4.11	U_Zr = 0.14	SnC-216	U_C = 1.99	U_Sn = 0.18
LiBr-225	U_Br = 6.72	U_Li = 0.0	TiO2-225	U_O = 8.3	U_Ti = 0.12
LiCl-225	U_Cl = 7.66	U_Li = 0.0	ZnO-216	U_O = 7.05	U_Zn = 13.03
MgTe-186	U_Mg = 0.05	U_Te = 4.84	ZnO-225	U_O = 7.29	U_Zn = 13.39
AlN-216	U_Al = 0.06	U_N = 4.91	ZnSe-186	U_Se = 5.19	U_Zn = 15.25
AgBr-216	U_Ag = 8.2	U_Br = 2.9	ZrO2-225	U_O = 8.61	U_Zr = 0.05



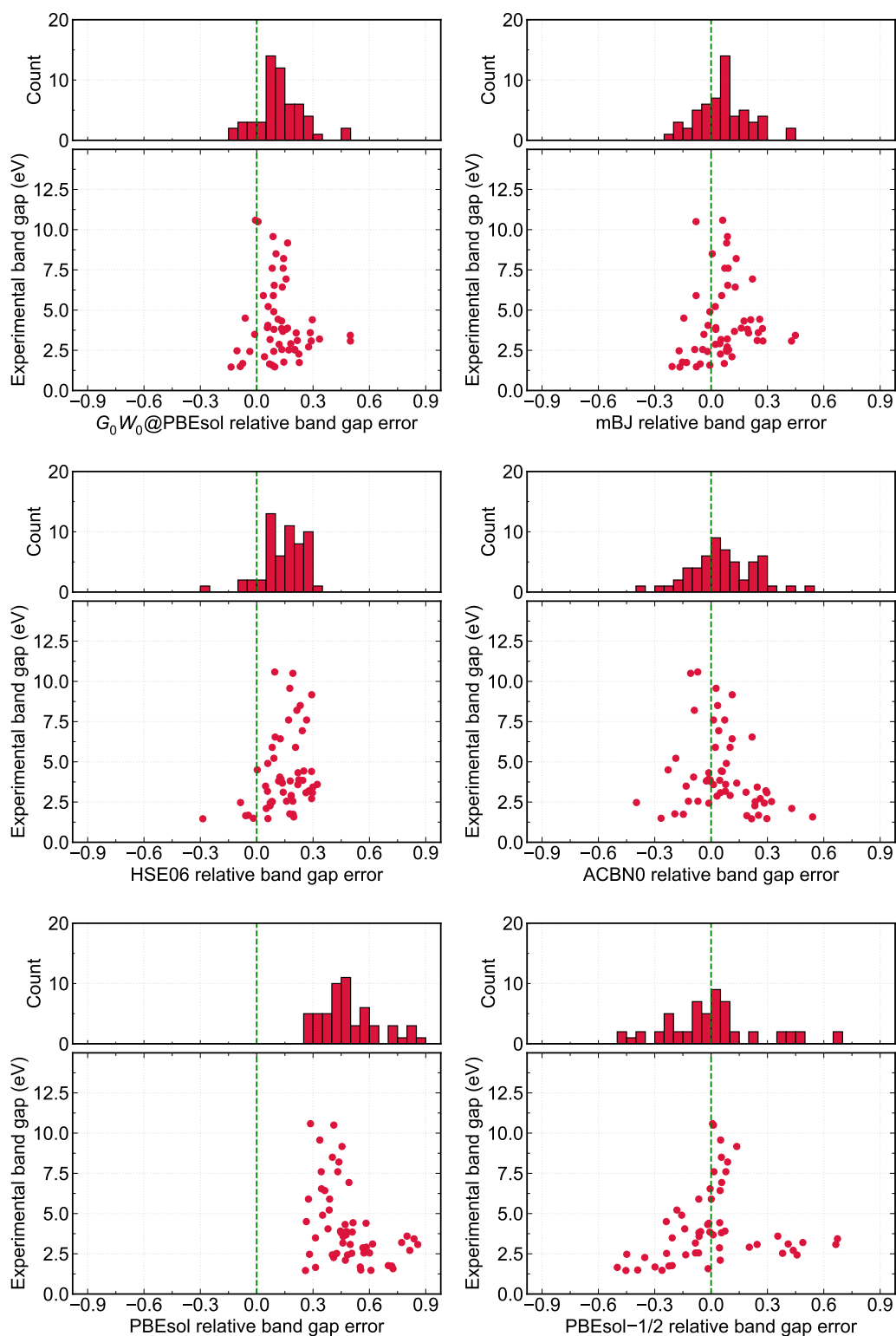
Supplementary Fig S1. Distribution histogram of differences between experimental and theoretical band gaps for (a) $G_0W_0@PBEsol$, (b) mBJ, (c) HSE06, (d) ACBN0, (e) PBEsol and (f) PBEsol-1/2.



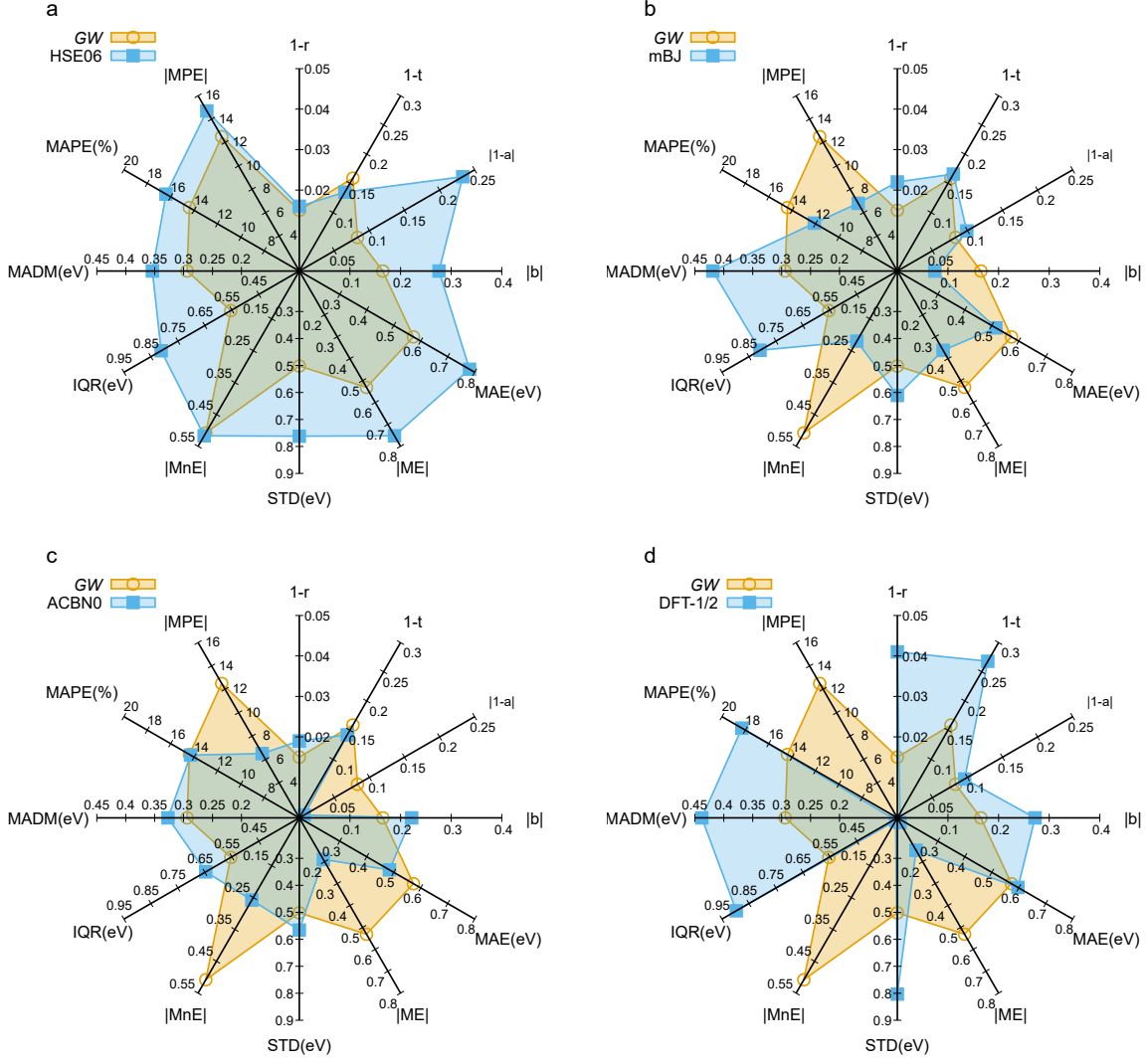
Supplementary Fig S2. Distribution histogram of differences between $G_0W_0@PBEsol$ and other theoretical methods: (a) HSE06, (b) mBJ, (c) ACBN0, and (d) DFT-1/2.



Supplementary Fig S3. Distribution histogram of differences between ACBN0 and other theoretical methods: (a) HSE06, (b) mBJ, (c) $G_0W_0@PBEsol$, and (d) DFT-1/2.



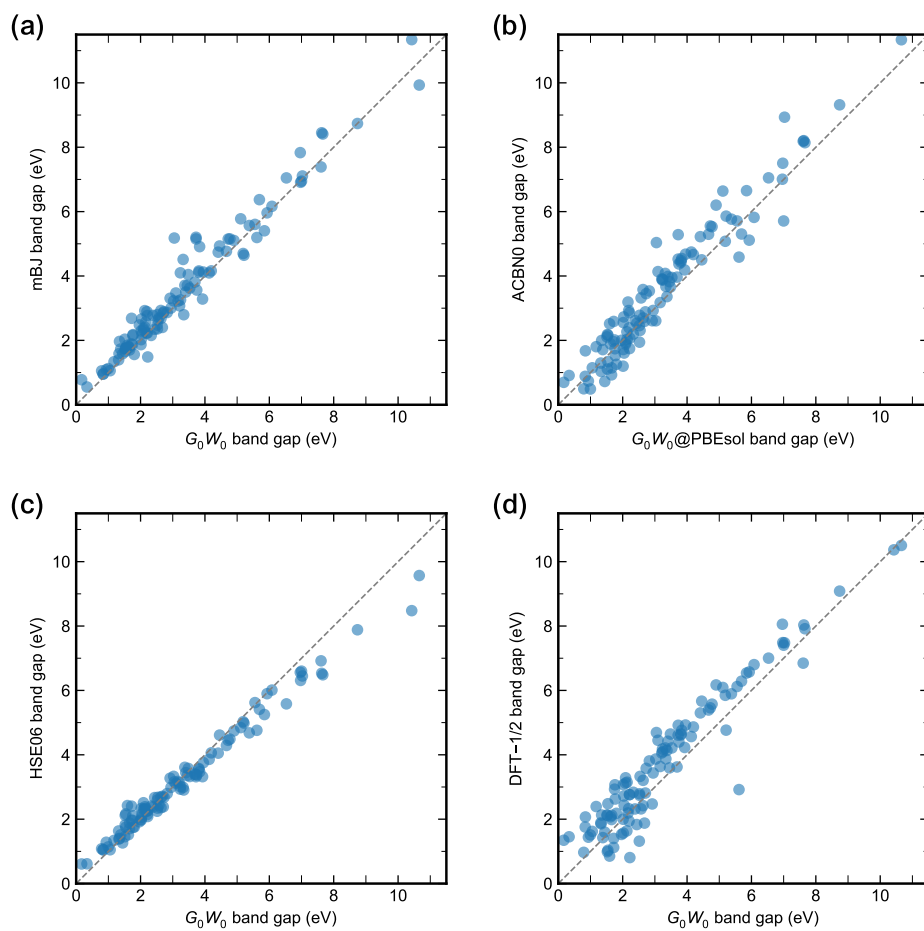
Supplementary Fig S4. The relative error between experimental and theoretical band gaps. Experimental band gap plotted as a function of the relative error for (a) G_0W_0 @PBEsol, (b) mBJ, (c) HSE06, (d) ACBN0, (e) PBEsol, and (f) PBEsol-1/2. The distribution histogram of the relative errors is also presented for each method. The dashed vertical green line corresponds to a zero error value.



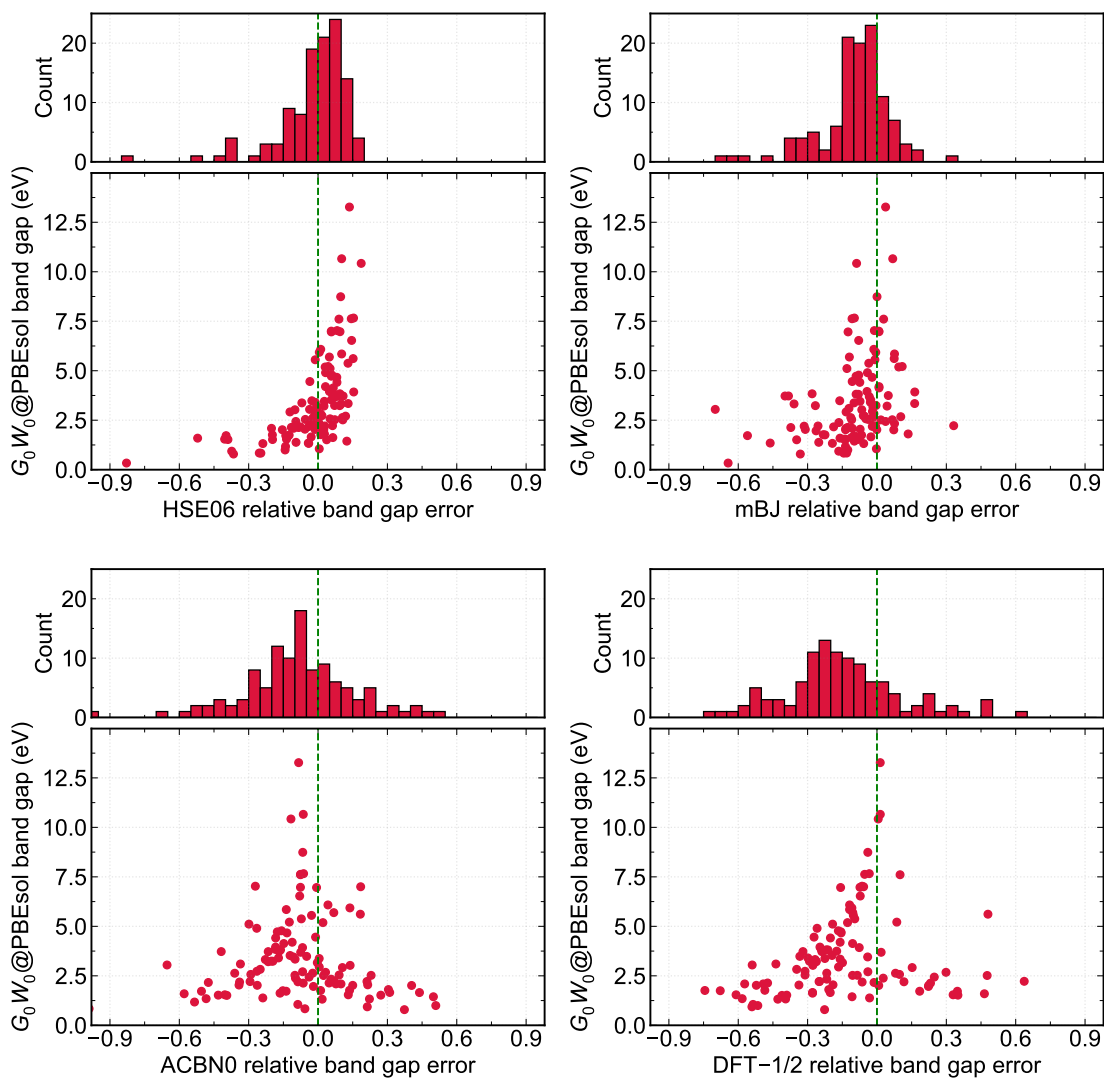
Supplementary Fig S5. Radar plots showing the statistical error quantities calculated in this benchmark study for (a) HSE06, (b) mBJ, (c) ACBN0, and (d) PBEsol–1/2. The values of the measures are summarized in Table I in the main text. For a better comparison, the radar plot corresponding to G_0W_0 @PBEsol error measures is shown in orange color in each plot.

TABLE S7. Statistical error measures of the calculated band gaps within different computational schemes, with respect to the experimental data for a subset after exclusion of the systems with a band gap larger than 7.0 eV. The blue and black colors show the best and the second-best values, respectively, selected with a slight tolerance (0.01 eV or 0.1%).

	PBEsol	mBJ	PBEsol–1/2	ACBN0	HSE06	G_0W_0 @PBEsol
Pearson r	89.4	0.928	0.868	0.936	0.959	0.951
Kendall τ	0.637	0.768	0.622	0.805	0.814	0.774
a	0.68	0.85	0.98	0.98	0.81	0.89
b (eV)	-0.56	0.22	0.04	-0.16	0.15	-0.08
ME (eV)	-1.65	-0.3	-0.05	-0.22	-0.51	-0.46
MPE (%)	-50.6	-6.8	0.6	-7.6	-13.4	-13.1
STD (eV)	0.66	0.53	0.79	0.52	0.43	0.44
MAE (eV)	1.65	0.44	0.58	0.45	0.54	0.51
MAPE (%)	50.6	12.8	20.6	15.8	15.6	15.3
MnE (eV)	-1.62	-0.17	0.08	-0.26	-0.49	-0.44
IQR (eV)	0.87	0.81	0.74	0.64	0.63	0.41
MADM (eV)	0.45	0.30	0.39	0.32	0.31	0.22
MaxAE	3.40	1.54	2.31	1.43	1.68	1.71



Supplementary Fig S6. Relationships between the quasi-particle band gap from the $G_0W_0@PBEsol$ calculation with (a) HSE06, (b) mBJ, (c) ACBN0, and PBEsol-1/2.



Supplementary Fig S7. The relative error between $G_0W_0@PBEsol$ and the band gaps that were obtained from other theoretical methods. $G_0W_0@PBEsol$ band gap plotted as a function of the relative error for (a) HSE06, (b) mBJ, (c) ACBN0, and (d) PBEsol-1/2. The distribution histogram of the relative errors is presented above each plot. The dashed vertical green line corresponds to a zero error value.

-
- [1] O. Madelung, *Semiconductors: data handbook* (Springer Berlin, Heidelberg, 2004).
- [2] A. Zoroddu, F. Bernardini, P. Ruggerone, and V. Fiorentini, First-principles prediction of structure, energetics, formation enthalpy, elastic constants, polarization, and piezoelectric constants of aln, gan, and inn: Comparison of local and gradient-corrected density-functional theory, *Phys. Rev. B* **64**, 045208 (2001).
- [3] I. Vurgaftman and J. R. Meyer, Band parameters for nitrogen-containing semiconductors, *Journal of Applied Physics* **94**, 3675 (2003).
- [4] J. Heyd, J. E. Peralta, G. E. Scuseria, and R. L. Martin, Energy band gaps and lattice parameters evaluated with the heyd-scuseria-ernzerhof screened hybrid functional, *The Journal of Chemical Physics* **123**, 174101 (2005).
- [5] H. Ott, Xi. die strukturen von mno, mns, agf, nis, snj₄, srcl₂, baf₂; präzisionsmessungen einiger alkalihalogenide, *Zeitschrift für Kristallographie - Crystalline Materials* **63**, 222 (1926).
- [6] R. Wyckoff, Interscience publishers, new york, new york rocksalt structure, *Crystal structures* **1**, 85 (1963).
- [7] P. Haas, F. Tran, and P. Blaha, Calculation of the lattice constant of solids with semilocal functionals, *Phys. Rev. B* **79**, 085104 (2009).
- [8] M. Piacentini, D. W. Lynch, and C. G. Olson, Thermoreflectance of lif between 12 and 30 ev, *Phys. Rev. B* **13**, 5530 (1976).
- [9] G. E. Jellison, L. A. Boatner, J. O. Ramey, J. A. Kolopus, L. A. Ramey, and D. J. Singh, Refractive index of sodium iodide, *Journal of Applied Physics* **111**, 043521 (2012).
- [10] D. Greenaway and R. Nitsche, Preparation and optical properties of group iv–vi₂ chalcogenides having the cdi₂ structure, *Journal of Physics and Chemistry of Solids* **26**, 1445 (1965).
- [11] W. Chen, G. Miceli, G.-M. Rignanese, and A. Pasquarello, Nonempirical dielectric-dependent hybrid functional with range separation for semiconductors and insulators, *Phys. Rev. Materials* **2**, 073803 (2018).
- [12] M. Cardona and M. L. W. Thewalt, Isotope effects on the optical spectra of semiconductors, *Rev. Mod. Phys.* **77**, 1173 (2005).
- [13] Y. Kaneko and T. Koda, New developments in iia–vib (alkaline-earth chalcogenide) binary semiconductors, *Journal of Crystal Growth* **86**, 72 (1988).
- [14] M. J. Weber, *Handbook of optical materials* (CRC press, 2018).
- [15] G. Baldini and B. Bosacchi, Optical properties of na and li halide crystals at 55 °k, *physica status solidi (b)* **38**, 325 (1970).
- [16] D. Roessler and W. Walker, Electronic spectrum of crystalline lithium fluoride, *Journal of Physics and Chemistry of Solids* **28**, 1507 (1967).